東京大学農学部演習林報告, 115, 1–36 (2006)

Soil loss in a forested watershed underlain by deeply weathered granite: comparison of observations to predictions of a GIS-based USLE

Krishna Bahadur KARKI*1 and Hirofumi SHIBANO*2

1. Introduction

Overview of Study

We used the Universal Soil Loss Equation (USLE) to predict soil loss in watersheds. The step-wise processes of the USLE applied in this study, i.e., soil loss prediction, model validation, and extension to a large watershed, are outlined in Figure 1. The major parameters of the soil loss prediction were watershed characteristics; the parameters used in the USLE were rainfall, soil, terrain, land use, and conservation practices, represented by factors of rainfall erosivity, soil erodibility, slope length and steepness, cover management, and support practices, respectively. Soil loss observations were conducted at the outlet of each small watershed to validate the

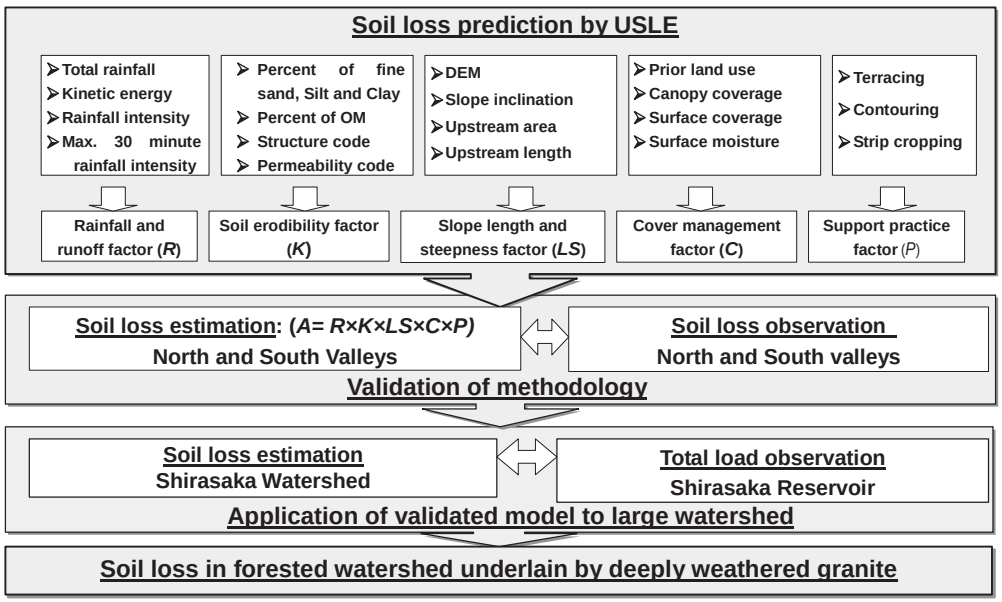

Fig. 1. Flow chart of soil loss study

*1 District Soil Conservation Office, Department of Soil and Watershed Management, Ministry of Forests and Soil Conservation, Government of Nepal
Department of Ecosystem Study, Graduate School of Agriculture and Life Sciences, The University of Tokyo (until 31 March, 2006)
*2 University Forest in Aichi, University Forests, Graduate School of Agricultural and Life Sciences, The University of Tokyo

prediction model. Finally, the validated model of soil loss was extended to the whole watershed to estimate soil loss in a mountainous region. Our observations and predictions of soil loss and discussion of the results reveal characteristics of forested watersheds underlain by deeply weathered granite.

1.1. Processes of soil loss

Soil erosion and sedimentation by water involve the processes of detachment, transport, and deposition of soil particles, and major forces include the impact of raindrops and the flow of water over the surface (RENARD *et al.* 1996). Splash, sheet, rill, and gully erosion are the classified steps from initial to advanced levels of water-induced erosion. Soil loss covers only the initial steps of soil erosion, such as splash, sheet (inter-rill), and rill erosion, which is a serious and continuous environmental degradation process resulting from erosion by water. In particular, sheet and rill erosion involves the detachment and transport of soil particles from topsoil layers, thereby degrading soil quality and reducing the productivity of the affected land (FERNANDEZ *et al.* 2003). The detachment of soil particles depends on rain-splash energy and particle entrapment, which is controlled by subsequent runoff that spreads more or less uniformly over the soil surface, and rill erosion caused by the scouring action of concentrated flow (KIMOTO 2003). Gully erosion occurs on lower slopes in steeper areas when rills continue to wash away, and becomes more severe as the quantity and intensity of rainfall in upland areas and runoff increase in channels downslope.

1.2. Short History of the USLE

Scientific planning for soil conservation and water management requires knowledge of the relationships among the factors that cause the loss of soil and water and those that help to reduce this loss (WISCHMEIER and SMITH 1978). Efforts to mathematically predict soil erosion by water were begun only about 50 years ago in the United States (RENARD *et al.* 1996). The USLE was developed in 1954 to estimate soil loss at the Runoff and Soil Loss Data Center of the Agricultural Research Service at Purdue University. It was first published in 1965, and this publication has served as the main reference manual for the USLE (WISCHMEIER and SMITH 1978). The USLE was originally developed for use on cropland, but it was also applied to rangeland and disturbed forestland in the early 1970s. Later, urban construction areas, recreational sites, highway embankments, and mine tailings were included among the applications of the USLE. KITAHARA *et al.* (2000) concluded that the USLE can be applied to estimate soil erosion for wide areas of long and steep slopes, including many kinds of cultivated and forested areas in Japan.

The USLE remains the most powerful, widely used and practical tool for estimating soil loss by sheet and rill erosion. The main reasons for its widespread application are its technical soundness and the lack of alternative models for programs of conservation planning to control soil erosion by water (RENARD *et al.* 1991). The USLE is an empirical model for predicting the average annual soil loss based on six risk factors (RENARD *et al.* 1991, KINNELL 1997, COHEN *et al.* 2005). Many revisions have been made to the USLE based on different requirements, and the

Revised Universal Soil Loss Equation (RUSLE) was introduced as an erosion model for the prediction of long-term average annual soil loss. This new model has been computerized to assist in calculations (RENARD *et al.* 1996). The combined use of Geographic Information Systems (GIS) and erosion models is an effective approach to estimate the magnitude and spatial distribution of erosion (MOLNAR and JULIAN 1997, FERNANDEZ *et al.* 2003, COHEN *et al.* 2005).

1.3. Parameters of the USLE

The rate of soil erosion in a particular location depends on soil type, climate, topography, cover management, and conservation efforts. Soil loss is caused by the dispersive action and transporting power of water, and it is affected by rainfall erosivity and soil erodibility. Rainfall erosivity is governed by rainfall characteristics, whereas soil erodibility is mainly a function of the physical properties and management of the soil (ODURO-AFRIYIE 1996). The USLE was primarily designed to predict erosion on straight slope sections, although FOSTER and WISCHMEIER (1974) developed a procedure to calculate the average soil loss on complex slope profiles by dividing an irregular slope into a limited number of uniform segments. Slope length as defined in the USLE is the distance from the origin of overland flow to the point at which the slope gradient decreases, deposition begins, or runoff enters a defined channel. The soil loss of a particular location increases with increasing slope length and steepness (WISCHMEIER and SMITH 1978, DESMET and GOVERS 1996, RENARD *et al*. 1996).

1.4. Applying the USLE to a forest

Forest cover types vary in the tree species, age, density, and ground vegetation, which can be disturbed by harvest operations, landslides, forest fires, or other disturbances at different times. At the same time, the development of canopy coverage also depends on microclimate, soil type, and disturbances. Therefore, the cover management factor for mountainous forests should be expressed as a function of time for each year after the evaluation of the changing conditions of the forest (KITAHARA *et al.* 2000). Soil and water conservation practices in forestlands are incorporated as the ‘support practice’ factor in the USLE and include retaining works, simple terracing, soil covering, and re-vegetation programs. In evaluating erosion control measures, it is necessary to determine the support practice factor of the USLE. The efficiency of such practices decreases with increased vegetation cover over time (KITAHARA *et al.* 2000).

1.5. Objective of this research

The main objectives of this study were to investigate soil loss in a forested watershed underlain by weathered granite and to validate a model for the estimation of soil loss from a forested watershed. Specifically, we attempted to: determine soil loss in two small catchments and one large watershed; assess the applicability of prediction methodology by comparing observed and predicted soil loss in small paired catchments; and, establish the proportion of soil lost to other kinds of erosion in a large watershed by comparing predicted soil loss and sediment deposition in a reservoir.

2. Site Description

The Shirasaka Watershed is one of the experimental watersheds in the University Forest in Aichi, the University of Tokyo. The area of this watershed is 88.6 ha, and it is located in Seto, Aichi Prefecture, Japan (35°12' N, 137°10' E; Figure 2). The average inclination of the watershed slope was 25°, with the major aspect directed to the northwest. The altitude ranged from 294 m at the outlet of the watershed to 629 m at the summit of Mt. Sanage. The watershed geology of Shirasaka is deeply weathered granite, and the climate is warm-humid with an annual precipitation of about 1800 mm. Before the establishment of the University Forest, this area was almost denuded because of fuelwood consumption by the ceramics industry. The implementation of soil erosion counter-measures with reforestation began in the early twentieth century. At present, this watershed is covered by dense forest (SHIBANO 1998).

A vegetation survey of the Shirasaka Watershed was conducted in 1996 (SHIBANO 1998), at which time a mixed coniferous and broadleaved forest comprised of akamatsu (Japanese red pine, *Pinus densiflora*), konara (Japanese oak, *Quercus serrata*), hinoki (Japanese cypress, *Chamaecyparis obtusa*), ryoubu (*Clethra barbinervis*), and akagashi (Japanese evergreen oak, *Quercus acuta*) formed the canopy layer, with a tree height of 14–18 m. The mid-story was composed of broadleaved trees, such as soyogo (long-stalk holly, *Ilex pedunculosa*), siromoji (*Lindera triloba*), asebi (Japanese pieris, *Pieris japonica*), inutsuge (Japanese holly, *Ilex crenata*),

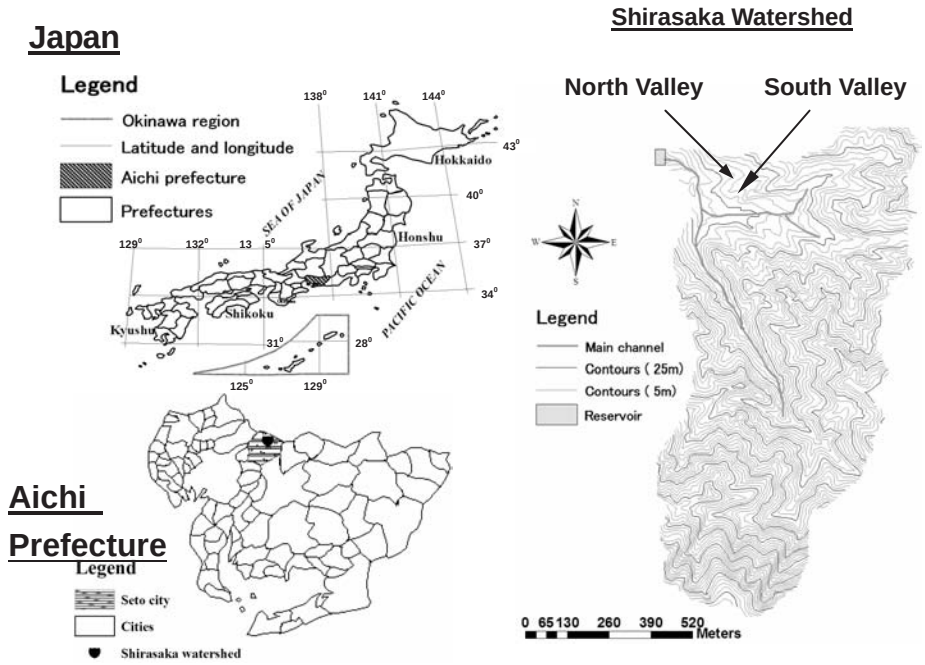

Fig. 2. Location and watersheds

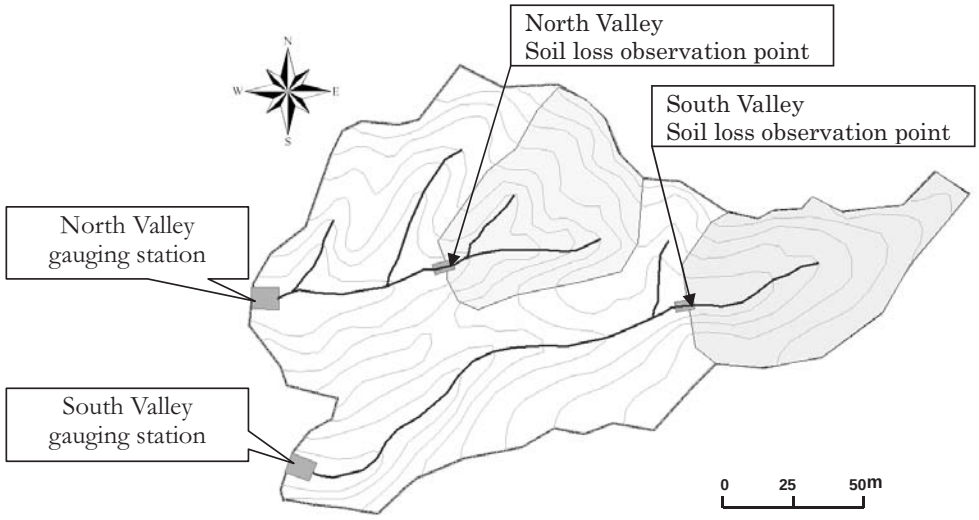

Fig. 3. Locations of soil loss observation points in the North and South Valleys

shirakashi (*Quercus myrsinaefolia*), and hisakaki (*Eurya japonica*). Akamatsu and konara trees were about 20 m tall and 40 cm in diameter on the gentle slope near the valley of the main stream (ARIYAKANON *et al.* 2000).

North Valley and South Valley are small paired catchments of the Shirasaka Watershed and are located at the northern edge among rough hills. The location of the North and South Valleys, including the stream-gauging stations and soil loss observation points, are shown in Figure 3. Many physical characteristics, such as geology, landform, vegetation, and soil type, are similar between the two valleys because of their proximity to each other, and the surface areas of these valleys are 0.44 and 0.48 ha, respectively. These small paired catchments were established for hydrological observations in the 1950s, and the measurement of surface and subsurface flow was the major objective at these sites. Therefore, stream gauging for hydrological studies has continued at the outlet of each valley since 1955 (YAMAGUCHI 1963), and we attached a soil loss observation facility to each station in 2001. The main parts of our stations for soil loss measurements were composed of an upper silting terrace, a middle silting ditch, and a lower silting reservoir (see section 3.2.1 for details). We observed soil loss from these small paired catchments between 9 August 2001 and 8 August 2005.

Soil loss observations in these valleys were conducted satisfactorily throughout the study period. However, a small disturbance occurred in September 2004 because of the maintenance of a trail in the upstream area of the observation point in the South Valley. The length of the improved footpath was <30 m, and the disturbed soil was estimated to be at most ~3 m^3, including drainage improvement work along the path. The disturbed soil was never artificially transported out of this catchment and was thought to have drained into the observation point more

rapidly than if it had not been disturbed.

3. Methodology

Several models are used to predict soil erosion using various expressions concerning erosion processes. Among these, the USLE is the simplest mathematical model that has been used worldwide since the 1960s (WISCHMEIER and SMITH 1978). This empirical model can be used to estimate average annual soil loss from specific field slopes under a specified land use and management system (RENARD *et al.* 1991). Therefore, we used the USLE to predict soil loss in the selected watersheds, and soil loss and sediment observations of the watersheds were conducted manually at the outlet of each catchment to evaluate the model.

3.1. Soil loss prediction

We examined the process of surface soil erosion in small to large watersheds using the USLE (WISCHMEIER and SMITH 1965) to estimate soil loss. For the analysis of slope length and steepness, the USLE used the concept of grid images connected by a channel network and integrated into the whole watershed to predict the spatial soil loss distribution of each location (DESMET and GOVERS 1996). The connected grid images are shown as a Digital Elevation Model (DEM) of the small paired catchments in Figures 4 (Figure 16 for Shirasaka Watershed with explanation in section 3.13). The other parameters of the USLE, such as the rainfall erosivity factor, soil erodibility factor, cover management factor, and support practice factor, are described below.

$$A = R \times K \times LS \times C \times P \qquad (3.1)$$

where A: soil loss for the time period concerned [ton ha^{-1}]
R: rainfall and runoff factor [MJ mm ha^{-1} hr^{-1}]
K: soil erodibility factor [ton ha hr ha^{-1} MJ^{-1} mm^{-1}]
LS: slope length and steepness factor [unitless]
C: cover management factor [unitless]
P: support practice factor [unitless]

The required information for the above factors of rainfall, soil characteristics, topography, land use, and conservation work in the watershed was collected from different sources, such as published literature, maps, and laboratory experiments. A description of each factor in the USLE is provided below.

3.1.1. Rainfall and runoff factor (*R*)

Soil erosion is closely related to rainfall through the detaching power of raindrops striking the soil surface and the contribution of rain to runoff (MORGAN 1996). The rainfall and runoff factor of the USLE indicates that when factors other than rainfall are held constant, soil losses from cultivated land are directly proportional to rainstorm parameters (WISCHMEIER and SMITH 1978). Moreover, the degree of severity of soil erosion depends on rainfall and local soil

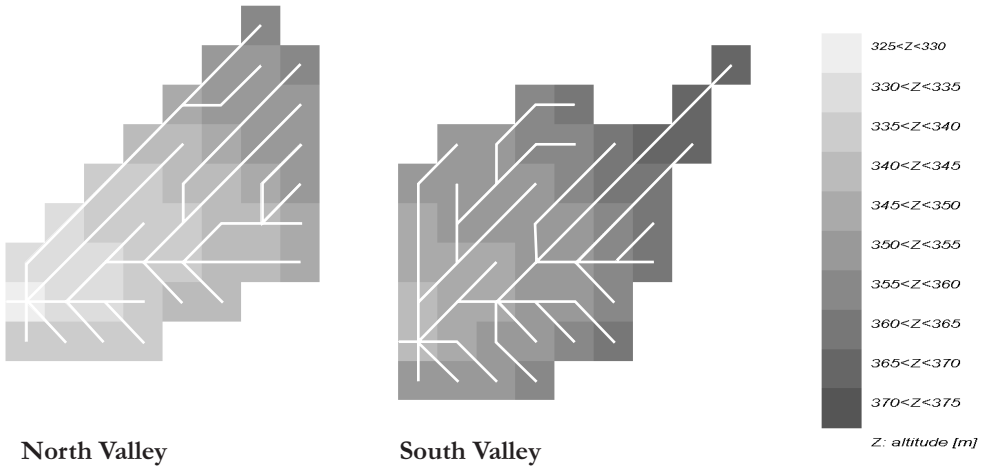

Fig. 4. Overland flow direction and shape of soil loss observation catchments of the North and South Valleys expressed with 10 × 10-m grids

characteristics. The stepwise estimation process for the rainfall and runoff factor is as follows.

1) Rainfall ($p(j)$) : 5-min rainfall in a time series during one event [mm]
2) One rainfall event (P_i) : total rainfall of the ith event [mm]

$$P_i = \sum_{j=1}^{k} p(j) \qquad (3.2)$$

where k was the number of 5-min rainfall in the ith event.

When P_i was less than 13 mm, the data were discarded, although they were used if at least 6 mm of rain fell within a 15-min period during that event.

3) Kinetic energy (KE) : rainfall kinetic energy [MJ ha^{-1} mm^{-1}]

$$KE = 0.119 + 0.087 \log_{10}(I) \quad I < 76 \text{ mm hr}^{-1} \qquad (3.3)$$

$$KE = 0.283 \quad I \geq 76 \text{ mm hr}^{-1} \qquad (3.4)$$

where I [mm hr^{-1}] is the average rainfall intensity for that period.

4) Rainfall factor (R) : total summation including all events during an arbitrary study period (e.g., 1 year, 4 years) [MJ mm ha^{-1} hr^{-1}]

$$R = \sum_{i=1}^{n} (I_m)_i (KE)_i P_i \qquad (3.5)$$

Where $(I_m)_i$ is the maximum 30-min rainfall intensity [mm hr^{-1}] for the ith event of the nth storm, and $(KE)_i$ is the kinetic energy of the ith event of the same nth storm.

In this study, we collected rainfall data every 5 min using an automatic digital data recorder. The rainfall recorder was located near the outlet of the Shirasaka Watershed. The total rainfall for

each event (P_i) and kinetic energy (*KE*) were calculated using equations (3.2) and (3.3), respectively. The 30-min rainfall intensity (I_{30}) was selected from the highest rainfall portion of the 5-min time series data during a rainfall event. Equation (3.5) was used to estimate the rainfall and runoff factor, *R*. Based on these calculations, the total number of rainfall events used over 4 years was 132, and the annual average rainfall factor *R* was 4568 MJ mm ha^{-1} hr^{-1} for these watersheds. A comparison of maximum 30-min rainfall intensity, rainfall events used, total rainfall, and the *R*-factor of each event is shown in Figure 5 for the whole study period.

3.1.2. Soil erodibility factor (*K*)

Soil erodibility is the inherent susceptibility of soil to be lost to erosion, which is one of the factors that affects the likelihood and severity of soil erosion. Soil erodibility is also a function of diverse soil properties, including particle size composition, stability of aggregates, shear strength, permeability, organic matter content, and chemical composition (MORGAN 1996). This is an experimentally determined quantitative value for a particular soil, which is the rate of soil loss per erosion index unit as measured on a "unit plot". A unit plot is 22.13 m long with a uniform length slope of 9% gradient in continuous fallow and tilled up and down the slope. Continuous fallow for this purpose refers to land that has been tilled and kept free of vegetation for more than 3 years (WISCHMEIER and SMITH 1978).

The erodibility of a soil as a material with a greater or lesser degree of coherence is defined by

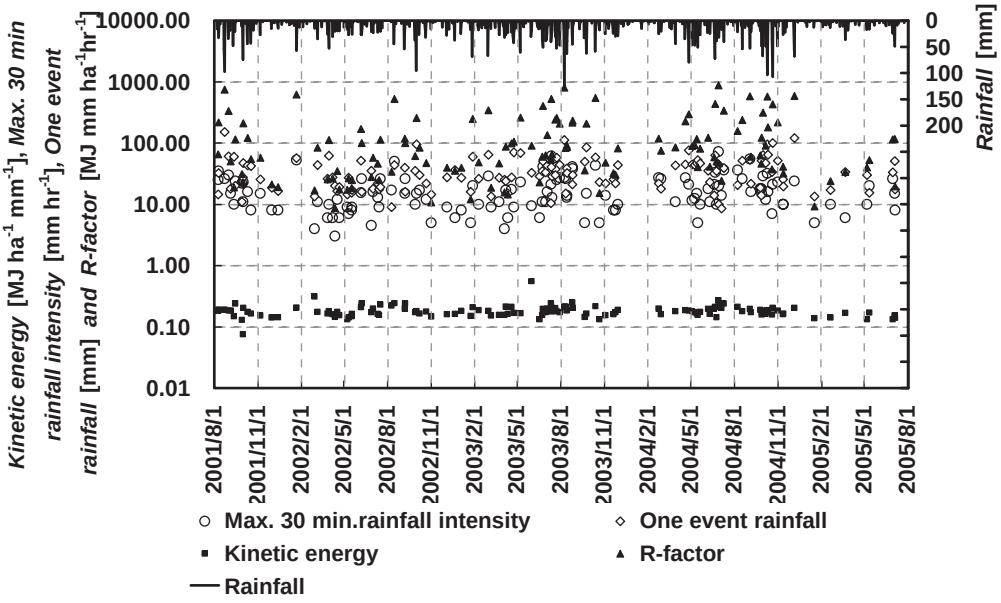

Fig. 5. Comparison of daily rainfall, *R*-factor, one rainfall event suitable for *R*-factor calculation, maximum 30-minute rainfall intensity, and kinetic energy at a weather station near the Shirasaka Reservoir

its resistance to two energy sources: the impact of raindrops on the soil surface and the shearing action of runoff between clods in inter-rills or rills. The soil erodibility factor *K* can be expressed as:

$$K = 2.8 \times 10^{-7} M^{1.14}(12 - OM) + 0.0043(S - 2) + 0.0033(P - 3) \quad (3.6)$$

$$M = (100 - Cl) \times Si$$

where

K : soil erodibility factor [ton hr MJ^{-1} mm^{-1}]
M : particle size parameter
Cl : percent of clay
Si : percent of silt plus very fine sand
OM : percent of organic matter
S : soil structure code
P : permeability code

Very fine sand (0.05–0.1 mm) and silt (0.002–0.05 mm) are more vulnerable to soil erosion within the group of sand and silt (0.002–2 mm), and their percentage is indicated by *Si*. The next fraction of soil texture is clay, indicated by *Cl* (<0.002 mm). Soil erodibility *K* is a function of the percentage of organic matter *OM*, *Si*, and *Cl*, as well as a code value of soil structure *S* and permeability class code *P*. The *K*-factor of the Shirasaka Watershed was calculated using equation (3.6) and the soil characteristics data are given in Table 1.

Based on the soil textural classification of these watersheds (MOROTO *et al.* 1978), the codes of soil structure and soil permeability were defined by adopting the soil structure and permeability table of WISCHMEIER and SMITH (1978). The calculated *K*-factor based on the soil characteristics of these watersheds was 0.0188 ton hr MJ^{-1} mm^{-1}.

3.1.3. Slope length and steepness factor (*LS*)

A grid can easily be generated using GIS and contour maps. We established a computational method to calculate slope attributes within any watershed, where slopes are not simple and have a structure connected by a flow line along a valley. Every grid within the watershed can be interpreted as a single segment of the mountain slope. Usually in a segment (an arbitrary grid) in

Table 1. Parameters of soil characteristics for *K*-factor in the North and South Valleys and the Shirasaka Watershed

Soil characteristics	Unit	Quantity
1. Fine sand and silt	Percent	33.7
2. Clay	Percent	2.3
3. Organic matter	Percent	5.8
4. Soil structure class (Coarse granular)	Code	3
5. Soil permeability (Moderate to rapid)	Code	2

Source: A-horizon samples from middle points on mountain slopes of the Shirasaka Watershed (after MOROTO *et al.* 1978)

the lower part of a long slope, soil loss increases if the slope has a constant inclination. However, slopes in mountainous areas have a complicated form, and the inclination changes from point to point. To understand the spatial distribution of soil loss, a systematic method using GIS must be introduced. We used the method proposed by DESMET and GOVERS (1996). It was necessary to make modifications and improvements to this method with respect to the theoretical validity and realistic conditions for its application. Here, we follow the methodology of these researchers and discuss the modifications to their methodology later.

Originally, the length factor L was defined as follows for simple slopes (FOSTER and WISCHMEIER 1974):

$$L = \left(\frac{\lambda}{22.13}\right)^{m} \tag{3.7}$$

where λ [m] is slope length, m is a slope length exponent, and the slope has a catchment area U [m^2]. m has values of 0.5 for slope steepness factor $S > 5$, 0.4 for $3 < S < 5$, 0.3 for $1 < S < 3$, and 0.2 for $S < 1$. The slope steepness factor is discussed later.

When a slope is divided into N segments of equal λ/N length, each L factor is calculated as follows, where k is an integer that indicates the position from the top of the catchment boundary.

$$L_k = (k^{m+1} - (k-1)^{m+1})\left(\frac{\lambda/N}{22.13}\right)^{m} = \frac{\left(k\frac{\lambda}{N}\right)^{m+1} - \left((k-1)\frac{\lambda}{N}\right)^{m+1}}{\frac{\lambda}{N}(22.13)^{m}} \tag{3.8}$$

Equation (3.8) leads to the estimation of soil loss from each segment in terms of ton ha^{-1} after multiplying other factors by the catchment area U/N [m^2].

$$L = \frac{1}{N}\sum_{k=1}^{N} L_k = \frac{1}{N}\frac{\left(N\frac{\lambda}{N}\right)^{m+1} - \left(0\frac{\lambda}{N}\right)^{m+1}}{\frac{\lambda}{N}(22.13)^{m}} = \left(\frac{\lambda}{22.13}\right)^{m} \tag{3.9}$$

Equation (3.8) can be easily modified into the following equation (3.10), which was developed by FOSTER and WISCHMEIER (1974). In this equation, λ_k is defined as the distance [m] from the lower boundary of the k-th segment to the upslope field boundary.

$$L_k = \frac{\lambda_k^{m+1} - \lambda_{k-1}^{m+1}}{(\lambda_k - \lambda_{k-1})(22.13)^{m}} \tag{3.10}$$

Before introducing the computational method, it is necessary to provide a short explanation of the single- and multiple-flow concepts. The former sets the downward flow direction into a single adjacent grid, whereas the latter allows multiple downward flow directions from a center grid into multiple adjacent grids.

We used a single-flow algorithm. The main reason for adopting the single-flow concept was based on the fact that a lower channel area can be depicted continuously and seems to be very natural. And the difference of this result can be seen clearly in their article. We can easily exclude the lower channel area using a single-flow algorithm. River bed erosion or sediment transport

occurs by hydraulic forces of water flow along the stream. This force is beyond the scope of the USLE methodology, and this point is specified in the Revised Universal Soil Loss Equation (RUSLE).

With respect to the computational method of DESMET and GOVERS (1996), we attempted to follow their method based on our interpretation. Similar to the multiple-flow algorithm presented by DESMET and GOVERS (1996), we calculated u_k, the fraction draining from upstream neighbors into the focal grid k, which is expressed below, where U is the upslope area available for inflow into grid k, including the focal grid k itself, contributing to outflow into the adjacent lower grid, and w_l is a weight factor from each neighbor l. In the single-flow algorithm, there is only one adjacent lower grid. U_k is interpreted as the upslope area multiplied by the ratio of channel length within the kth grid to the total channel length within the upslope area U and grid k:

$$u_k = U\frac{2Dw_k}{\sum_{l=1}^{k} 2Dw_l} = U\frac{w_k}{\sum_{l=1}^{k} w_l} \tag{3.11}$$

where $w_l = \frac{1}{2}$ for a cardinal direction from or toward neighbor l,

$w_l = \frac{\sqrt{2}}{2}$ for a diagonal direction from or toward neighbor l.

This equation can be transformed as follows:

$$\frac{1}{\rho_k} \equiv \frac{u_k}{Dw_k} = \frac{U}{D\sum_{l=1}^{k} (\sin\alpha_l + \cos\alpha_l)} \tag{3.12}$$

where we rewrite w_k as x_k as follows;

$$x_k \equiv \sum_{j=1}^{k} (\sin\alpha_j + \cos\alpha_j) \tag{3.13}$$

The denominator of equation (3.12) indicates the total length of the channel network of the upslope drainage basin expressed as Dx_k. This is the same as λ_k [m], the slope distance from the lower boundary of the kth segment to the upslope field boundary.

$$\lambda_k \equiv Dx_k = \rho_k U \tag{3.14}$$

In a grid-based DEM, the surface is subdivided into square grid cells. The one-dimensional expression above can be replaced with a two-dimensional expression. Therefore, we can easily derive the following equation by substituting λ_k into equation (3.10) after replacing λ_k with λ_{ij}, where Dx_{ij} represents the total channel length and $Dx_{ij}/U_{i,j}$ is the value of the total channel network length divided by the upstream drainage area, i.e., drainage density. U_{ij}/Dx_{ij} is the reciprocal value of drainage density, i.e., the average slope width susceptible to sheet or rill erosion. As a result, the higher the stream density is, the narrower the slope width becomes.

$$L_{ij} = \frac{(\rho_{ij}U_{ij})^{m+1} - (\rho_{ij}(U_{ij} - D^2))^{m+1}}{(\rho_{ij}U_{ij} - \rho_{ij}(U_{ij} - D^2))(22.13)^m} = \frac{U_{i,j}{}^{m+1} - (U_{i,j} - D^2)^{m+1}}{(1/\rho_{ij})^m D^2 (22.13)^m} \quad (3.15)$$

$$\lambda_{ij}/D \equiv x_{ij} = \sum_{i,j}^{N} (\sin\alpha_{ij} + \cos\alpha_{ij}) \quad (3.16)$$

For example, in the case of South Valley, D was set to 10 m and the total drainage area was 4800 m^2, and each topographic factor can be specified in the following figures. Figure 4 shows the altitude distribution on a topographic map of North Valley and South Valley in a grid image. We established the observation sites of surface soil erosion in both valleys because these observation sites were located at the lower part of the springs, i.e., small water sources with defined channels. The springs eroded the channel until the issued water reached the observation facilities. However, the springs were located only about 5 m apart upstream from the observation point, and their discharge was small and stable. We therefore assumed that the water from the springs had only a small effect on streambed erosion. Therefore, most of the sediment observed at the site was considered surface soil erosion.

The lowest grids of both catchments are surrounded by a thick line (Figure 6). Soil loss observation sites were established here. Using a computational procedure, these two grids were

0	350	350	351	355	0	0	0	0	0	0	0	0	0	0	0	0	0	0	0
347	347	347	348	350	352	354	355	0	0	0	0	0	0	0	0	0	0	0	0
344	344	345	346	347	348	352	354	355	0	0	0	0	0	0	0	0	0	372	373
339	339	342	343	342	345	350	353	354	355	355	0	0	0	356	361	0	0	369	370	370
337	338	339	339	340	344	348	350	353	352	352	354	354	354	355	358	362	365	367	366	364
336	336	336	337	338	341	344	347	352	349	350	352	353	353	354	356	360	363	366	364	359
332	333	334	336	337	338	340	342	348	347	348	349	350	352	353	354	358	361	364	360	357
330	331	333	334	335	337	340	342	345	345	345	346	347	349	350	352	356	360	364	358	355
329	329	332	334	338	340	342	343	344	344	344	344	345	347	350	354	358	362	360	356	353
331	335	335	338	339	340	340	340	339	340	343	343	348	352	354	358	360	360	356	353	351
333	335	337	338	337	336	336	336	339	343	346	350	352	354	356	357	358	356	352	350	348
335	336	336	334	334	334	336	340	343	346	349	352	354	354	354	354	354	352	349	347	346

Fig. 6. DEM of the North and South Valleys and surrounding areas
Note: The number in each grid indicates the elevation [m]. The grid surrounded by a thick line is the lowest grid.

0	50	50	50	50	0	0	0	0	0	0	0	0	0	0	0	0	0	0	0
50	50	60	60	50	50	60	60	0	0	0	0	0	0	0	0	0	0	0	0
50	50	60	50	50	60	60	60	60	0	0	0	0	0	0	0	0	0	60	40
60	60	50	50	60	60	70	60	60	50	50	0	0	0	60	70	0	0	60	40	50
60	50	50	60	60	60	60	60	60	50	60	60	60	50	60	70	60	60	60	40	50
50	50	60	60	60	50	60	50	60	50	60	50	50	60	60	60	60	60	40	30	40
60	60	60	60	60	60	60	70	70	50	50	50	50	60	50	60	60	60	40	40	50
60	50	60	60	70	70	70	70	70	50	50	50	60	60	60	70	70	70	30	40	40
70	70	70	70	70	80	80	50	50	50	60	50	60	70	70	70	80	40	40	40	40
80	10	80	80	80	50	50	50	60	70	70	70	70	10	80	80	80	40	40	40	50
80	80	40	50	50	50	60	70	70	70	80	10	80	80	80	50	40	40	40	50	40
80	80	40	50	60	60	60	10	80	80	80	80	40	50	50	50	50	30	40	40	30

Fig. 7. Flow direction from the focal grid to the adjacent lower grid in the North and South Valleys. Note: 10 represents north, 20 represents northeast, 30 represents east, …, 80 represents northwest.

0	1	1	1	1	0	0	0	0	0	0	0	0	0	0	0	0	0	0	0
1	2	2	2	2	1	1	1	0	0	0	0	0	0	0	0	0	0	0	0
3	5	3	1	3	3	2	1	1	0	0	0	0	0	0	0	0	0	1	2
4	9	1	2	7	5	2	2	1	1	1	0	0	0	2	1	0	0	2	1	1
10	1	2	10	6	1	3	2	1	2	2	1	1	3	2	1	1	3	1	1	3
1	2	13	7	2	4	3	2	1	5	2	2	1	6	1	2	4	2	1	1	6
2	16	8	3	1	8	6	5	1	8	1	3	8	2	3	5	3	1	1	2	1
17	9	4	23	21	11	3	2	1	9	2	4	11	1	17	8	3	1	1	3	4
45	44	28	3	1	1	1	1	1	10	3	16	27	25	4	2	1	1	1	1	4
2	1	1	1	1	1	1	2	67	65	49	48	2	2	1	1	1	1	2	2	2
2	1	1	1	1	2	78	76	4	2	2	1	1	1	1	1	1	1	2	3	5
1	1	1	3	2	81	5	1	1	1	1	1	1	1	1	2	1	2	4	6	1

Fig. 8. Upstream drainage area [$\times$ 100m^2] of a focal grid including the focal grid itself in the North and South Valleys.
Note: These values are expressed as U_{ij} /100

0	10	10	10	10	0	0	0	0	0	0	0	0	0	0	0	0	0	0	0
10	20	24	24	20	10	14	14	0	0	0	0	0	0	0	0	0	0	0	0
34	54	38	10	30	38	28	14	14	0	0	0	0	0	0	0	0	0	14	28
48	106	10	20	82	66	24	28	14	10	10	0	0	0	24	10	0	0	28	14	10
120	10	20	116	80	14	42	28	14	20	24	14	14	34	24	10	14	42	14	14	34
10	20	150	94	28	52	42	24	14	54	28	24	10	72	14	28	56	28	14	10	72
24	184	108	42	14	108	72	58	10	92	10	34	92	28	38	70	42	14	14	28	10
198	118	56	287	259	126	30	20	10	102	20	44	134	14	223	100	34	10	10	38	52
565	555	346	34	10	14	14	10	10	112	34	188	348	320	48	24	14	14	14	14	52
28	10	14	14	14	10	10	20	814	790	605	595	24	24	14	14	14	14	28	28	24
28	14	14	10	10	20	941	917	48	24	28	10	14	14	14	10	14	14	28	38	66
14	14	14	34	24	975	58	10	14	14	14	14	14	10	10	20	10	24	52	80	10

Fig. 9. Upstream channel length including the reach to the adjacent lower grid in the North and South Valleys.
Note: These values are equal to λ_{ij} [m]

0.0	10.0	10.0	10.0	10.0	0.0	0.0	0.0	0.0	0.0	0.0	0.0	0.0	0.0	0.0	0.0	0.0	0.0	0.0	0.0
10.0	10.0	8.3	8.3	10.0	10.0	7.1	7.1	0.0	0.0	0.0	0.0	0.0	0.0	0.0	0.0	0.0	0.0	0.0	0.0
8.8	9.3	7.9	10.0	10.0	7.9	7.1	7.1	7.1	0.0	0.0	0.0	0.0	0.0	0.0	0.0	0.0	0.0	7.1	7.1
8.3	8.5	10.0	10.0	8.5	7.6	8.3	7.1	7.1	10.0	10.0	0.0	0.0	0.0	8.3	10.0	0.0	0.0	7.1	7.1	10.0
8.3	10.0	10.0	8.6	7.5	7.1	7.1	7.1	7.1	10.0	8.3	7.1	7.1	8.8	8.3	10.0	7.1	7.1	7.1	7.1	8.8
10.0	10.0	8.7	7.4	7.1	7.7	7.1	8.3	7.1	9.3	7.1	8.3	10.0	8.3	7.1	7.1	7.1	7.1	7.1	10.0	8.3
8.3	8.7	7.4	7.1	7.1	7.4	8.3	8.6	10.0	8.7	10.0	8.8	8.7	7.1	7.9	7.1	7.1	7.1	7.1	7.1	10.0
8.6	7.6	7.1	8.0	8.1	8.7	10.0	10.0	10.0	8.8	10.0	9.1	8.2	7.1	7.6	8.0	8.8	10.0	10.0	7.9	7.7
8.0	7.9	8.1	8.8	10.0	7.1	7.1	10.0	10.0	8.9	8.8	8.5	7.8	7.8	8.3	8.3	7.1	7.1	7.1	7.1	7.7
7.1	10.0	7.1	7.1	7.1	10.0	10.0	10.0	8.2	8.2	8.1	8.1	8.3	8.3	7.1	7.1	7.1	7.1	7.1	7.1	8.3
7.1	7.1	7.1	10.0	10.0	10.0	8.3	8.3	8.3	8.3	7.1	10.0	7.1	7.1	7.1	10.0	7.1	7.1	7.1	7.9	7.6
7.1	7.1	7.1	8.8	8.3	8.3	8.6	10.0	7.1	7.1	7.1	7.1	7.1	10.0	10.0	10.0	10.0	8.3	7.7	7.5	10.0

Fig. 10. Average slope width (reciprocal value of drainage density) in the North and South Valleys.
Note: These values are equal to $1/\rho_{ij}$ [m]

set as outlet points of eroded soil. Therefore, we excluded these grids from the catchment domain. Figure 7 shows the flow direction of each grid. Based on the single-flow concept, flow was set in only one direction, but each grid could receive flow from adjacent grids in eight directions, with seven grids at maximum and none at minimum. Most grids on the ridge of the catchment and the boundary of the subcatchment had no neighboring grids upstream. Figure 8 shows the number of upstream grids relative to a focal grid. If the grid was located on a ridge or boundary of the subcatchment, the number reached unity, i.e., 1.

Figure 9 shows the upstream channel length λ_{ij} [m], and Figure 10 shows the average upslope width having values <10 m.

Figure 11 shows the *L*-factor, which indicates one of the aspects concerning erodibility, i.e., the lower part of a slope is likely to experience heavy water flow that will erode the soil surface. The *L*-factor can be interpreted as a hydrological condition affecting erosion. If we connect all grids with a channel network, the downstream area is considered highly erodible. Because it is unnatural for surface soil erosion to occur in grids with a large *L* value, we excluded such areas. A spring begins at the outlet of North Valley and South Valley. Therefore, the downstream part with an upstream area >5000 m^2 should be excluded. This condition is critical to the evaluation of soil loss.

The slope gradient for each point of the regular grid of the study area can usually be computed according to the following algorithm:

$$G_{ij} = \sqrt{G_x^{\,2} + G_y^{\,2}} \qquad (3.17)$$

Here, we chose a slope gradient in terms of $\sin\theta$, but we defined the slope gradient as an

0.0	0.7	0.7	0.7	0.7	0.0	0.0	0.0	0.0	0.0	0.0	0.0	0.0	0.0	0.0	0.0	0.0	0.0	0.0	0.0
0.7	1.2	1.3	1.3	1.2	0.7	0.8	0.8	0.0	0.0	0.0	0.0	0.0	0.0	0.0	0.0	0.0	0.0	0.0	0.0
1.7	2.2	1.8	0.7	1.6	1.8	1.5	0.8	0.8	0.0	0.0	0.0	0.0	0.0	0.0	0.0	0.0	0.0	0.8	1.5
2.1	3.2	0.7	1.2	2.8	2.5	1.3	1.5	0.8	0.7	0.7	0.0	0.0	0.0	1.3	0.7	0.0	0.0	1.5	0.8	0.7
3.4	0.7	1.2	3.3	2.7	0.8	1.9	1.5	0.8	1.2	1.3	0.8	0.8	1.7	1.3	0.7	0.8	1.9	0.8	0.8	1.7
0.7	1.2	3.8	3.0	1.5	2.1	1.9	1.3	0.8	2.2	1.5	1.3	0.7	2.6	0.8	1.5	2.2	1.5	0.8	0.7	2.6
1.3	4.3	3.2	1.9	0.8	3.2	2.6	2.3	0.7	3.0	0.7	1.7	3.0	1.5	1.8	2.5	1.9	0.8	0.8	1.5	0.7
4.4	3.4	2.2	5.3	5.1	3.5	1.6	1.2	0.7	3.1	1.2	2.0	3.6	0.8	4.7	3.1	1.7	0.7	0.7	1.8	2.1
7.5	7.5	5.9	1.7	0.7	0.8	0.8	0.7	0.7	3.3	1.7	4.3	5.9	5.6	2.1	1.3	0.8	0.8	0.8	0.8	2.1
1.5	0.7	0.8	0.8	0.8	0.7	0.7	1.2	9.1	8.9	7.8	7.7	1.3	1.3	0.8	0.8	0.8	0.8	1.5	1.5	1.3
1.5	0.8	0.8	0.7	0.7	1.2	9.7	9.6	2.1	1.3	1.5	0.7	0.8	0.8	0.8	0.7	0.8	0.8	1.5	1.8	2.5
0.8	0.8	0.8	1.7	1.3	9.9	2.3	0.7	0.8	0.8	0.8	0.8	0.8	0.7	0.7	1.2	0.7	1.3	2.1	2.7	0.7

Fig. 11. Length factor L_{ij} [unitless] in the North and South Valleys

0	287	287	287	447	0	0	0	0	0	0	0	0	0	0	0	0	0	0	0
287	287	248	248	371	371	390	207	0	0	0	0	0	0	0	0	0	0	0	0
319	319	303	287	371	384	333	272	140	0	0	0	0	0	0	0	0	0	207	272
335	334	287	330	354	409	364	240	272	287	287	0	0	0	305	447	0	0	240	390	514
174	196	287	264	272	390	390	333	390	287	248	272	140	119	215	287	390	303	272	443	395
371	242	234	207	272	369	390	419	577	230	240	215	287	149	140	303	362	303	390	447	373
292	234	207	174	207	297	201	448	514	199	287	287	261	240	248	333	362	333	390	365	196
207	201	240	149	211	257	242	242	287	148	196	242	277	272	241	340	358	371	514	362	247
99	288	257	302	371	333	333	287	447	242	188	168	203	323	388	381	390	390	443	333	272
272	514	390	390	333	371	371	330	261	288	148	327	419	364	443	492	390	492	390	390	310
240	272	207	371	287	287	177	288	370	381	390	573	536	390	272	287	390	443	402	340	297
272	207	333	290	248	158	240	371	443	443	390	390	272	371	447	410	447	340	333	256	196

Fig. 12. Inclination expressed in sine values multiplied by 1000 in the North and South Valleys

average of the inclination of the inflow and outflow direction through the focal grid. Therefore, the maximum number of flow directions in one grid was eight. We assumed that surface soil is transported only along the flow direction. If a grid received flow from three directions and flowed out in one direction, the slope gradient (Figure 12) was calculated as the average of four directions other than equation (3.17). This is because the measure is proportional to gravitational force on soil particles and tractive force by overland flow.

Using the sine value of every grid, it can be easily transformed into an *S* factor as shown in Figure 13. The transformation process is easily accomplished using the following equations.

$$S_{ij} = 10.8 \sin\theta_{ij} + 0.03 \quad \text{when} \quad \sin\theta_{ij} < 0.9 \tag{3.18}$$

$$S_{ij} = 16.8 \sin\theta_{ij} - 0.5 \quad \text{when} \quad \sin\theta_{ij} \geq 0.9 \tag{3.19}$$

The *L*-factor can again be shown in Figure 14, with the lower reaches of the stream shown as excluded parts in light grey. Figure 15 shows the *LS*-factor as a product of the *L*- and *S*-factors. In this case, grids with an upstream area >5000 m^2 or a gradient <0.05 of the sine value (assigned as deposition areas) were excluded.

We first confirmed the computational method for the slope length and steepness factor as experimental calculations for the small paired catchments, i.e., North and South Valleys. The method was then extended to the large Shirasaka Watershed. We noted several differences between the small paired catchments and the large watershed in the process of computation, including stream channel line or depositional area. These special grids showed very high or very low values of slope length as supply of overland flow and very low values of surface inclination (see Figures 20 and 21 explained later in the same section).

0.0	4.3	4.3	4.3	7.0	0.0	0.0	0.0	0.0	0.0	0.0	0.0	0.0	0.0	0.0	0.0	0.0	0.0	0.0	0.0
4.3	4.3	3.7	3.7	5.7	5.7	6.1	3.0	0.0	0.0	0.0	0.0	0.0	0.0	0.0	0.0	0.0	0.0	0.0	0.0
4.9	4.9	4.6	4.3	5.7	6.0	5.1	4.1	1.9	0.0	0.0	0.0	0.0	0.0	0.0	0.0	0.0	0.0	3.0	4.1
5.1	5.1	4.3	5.0	5.4	6.4	5.6	3.5	4.1	4.3	4.3	0.0	0.0	0.0	4.6	7.0	0.0	0.0	3.5	6.1	8.1
2.4	2.8	4.3	3.9	4.1	6.1	6.1	5.1	6.1	4.3	3.7	4.1	1.9	1.5	3.1	4.3	6.1	4.6	4.1	6.9	6.1
5.7	3.6	3.4	3.0	4.1	5.7	6.1	6.5	9.2	3.4	3.5	3.1	4.3	2.0	1.9	4.6	5.6	4.6	6.1	7.0	5.8
4.4	3.4	3.0	2.4	3.0	4.5	2.9	7.0	8.1	2.8	4.3	4.3	3.9	3.5	3.7	5.1	5.6	5.1	6.1	5.6	2.8
3.0	2.9	3.5	2.0	3.0	3.8	3.6	3.6	4.3	2.0	2.8	3.6	4.2	4.1	3.5	5.2	5.5	5.7	8.1	5.6	3.6
1.2	4.3	3.8	4.6	5.7	5.1	5.1	4.3	7.0	3.6	2.7	2.3	2.9	4.9	6.0	5.9	6.1	6.1	6.9	5.1	4.1
4.1	8.1	6.1	6.1	5.1	5.7	5.7	5.0	3.9	4.3	2.0	5.0	6.5	5.6	6.9	7.8	6.1	7.8	6.1	6.1	4.7
3.5	4.1	3.0	5.7	4.3	4.3	2.5	4.3	5.7	5.9	6.1	9.1	8.5	6.1	4.1	4.3	6.1	6.9	6.3	5.2	4.5
4.1	3.0	5.1	4.4	3.7	2.2	3.5	5.7	6.9	6.9	6.1	6.1	4.1	5.7	7.0	6.4	7.0	5.2	5.1	3.8	2.8

Fig. 13. *S*-factors in the North and South Valleys.

0.0	0.7	0.7	0.7	0.7	0.0	0.0	0.0	0.0	0.0	0.0	0.0	0.0	0.0	0.0	0.0	0.0	0.0	0.0	0.0
0.7	1.2	1.3	1.3	1.2	0.7	0.8	0.8	0.0	0.0	0.0	0.0	0.0	0.0	0.0	0.0	0.0	0.0	0.0	0.0
1.7	2.2	1.8	0.7	1.6	1.8	1.5	0.8	0.8	0.0	0.0	0.0	0.0	0.0	0.0	0.0	0.0	0.0	0.8	1.5
2.1	3.2	0.7	1.2	2.8	2.5	1.3	1.5	0.8	0.7	0.7	0.0	0.0	0.0	1.3	0.7	0.0	0.0	1.5	0.8	0.7
3.4	0.7	1.2	3.3	2.7	0.8	1.9	1.5	0.8	1.2	1.3	0.8	0.8	1.7	1.3	0.7	0.8	1.9	0.8	0.8	1.7
0.7	1.2	3.8	3.0	1.5	2.1	1.9	1.3	0.8	2.2	1.5	1.3	0.7	2.6	0.8	1.5	2.2	1.5	0.8	0.7	2.6
1.3	4.3	3.2	1.9	0.8	3.2	2.6	2.3	0.7	3.0	0.7	1.7	3.0	1.5	1.8	2.5	1.9	0.8	0.8	1.5	0.7
4.4	3.4	2.2	5.3	5.1	3.5	1.6	1.2	0.7	3.1	1.2	2.0	3.6	0.8	4.7	3.1	1.7	0.7	0.7	1.8	2.1
7.5	7.5	5.9	1.7	0.7	0.8	0.8	0.7	0.7	3.3	1.7	4.3	5.9	5.6	2.1	1.3	0.8	0.8	0.8	0.8	2.1
1.5	0.7	0.8	0.8	0.8	0.7	0.7	1.2			7.8	7.7	1.3	1.3	0.8	0.8	0.8	0.8	1.5	1.5	1.3
1.5	0.8	0.8	0.7	0.7	1.2			2.1	1.3	1.5	0.7	0.8	0.8	0.8	0.7	0.8	0.8	1.5	1.8	2.5
0.8	0.8	0.8	1.7	1.3		2.3	0.7	0.8	0.8	0.8	0.8	0.8	0.7	0.7	1.2	0.7	1.3	2.1	2.7	0.7

Fig. 14. *L*-factor excluding channel sections in the North and South Valleys.
"Channel sections" shown in light grey have upstream areas that exceed 50 grids (5000 m^2). Along such locations, gully and stream bed erosion occur that are beyond the scope of the USLE.

0.0	2.9	2.9	2.9	4.7	0.0	0.0	0.0	0.0	0.0	0.0	0.0	0.0	0.0	0.0	0.0	0.0	0.0	0.0	0.0
2.9	5.3	4.9	4.9	7.0	3.9	4.8	2.4	0.0	0.0	0.0	0.0	0.0	0.0	0.0	0.0	0.0	0.0	0.0	0.0
8.2	10.8	8.2	2.9	9.1	10.7	7.4	3.2	1.5	0.0	0.0	0.0	0.0	0.0	0.0	0.0	0.0	0.0	2.4	5.9
10.6	16.3	2.9	6.2	15.2	15.6	7.6	5.1	3.2	2.9	2.9	0.0	0.0	0.0	6.2	4.7	0.0	0.0	5.1	4.8	5.5
8.2	1.9	5.3	13.2	11.1	4.8	11.4	7.4	4.8	5.3	4.9	3.2	1.5	2.5	4.2	2.9	4.8	8.6	3.2	5.5	10.4
3.9	4.4	13.1	8.9	5.9	12.2	11.4	8.8	7.3	7.5	5.1	4.2	2.9	5.2	1.5	6.7	12.4	6.7	4.8	4.7	14.9
5.9	14.6	9.6	4.6	2.4	14.4	7.4	16.2	5.5	8.4	2.9	7.3	11.5	5.1	6.6	12.9	10.5	4.1	4.8	8.2	1.9
13.2	9.7	7.9	10.7	15.4	13.3	5.7	4.4	2.9	6.2	3.4	7.0	15.0	3.2	16.6	16.1	9.3	3.9	5.5	10.0	7.8
8.8	32.4	22.4	7.7	3.9	4.1	4.1	2.9	4.7	11.7	4.5	10.0	17.2	27.8	12.4	7.9	4.8	4.8	5.5	4.1	8.7
5.9	5.5	4.8	4.8	4.1	3.9	3.9	6.2			15.5	38.6	8.8	7.6	5.5	6.2	4.8	6.2	8.8	8.8	6.3
5.1	3.2	2.4	3.9	2.9	5.3			11.8	7.9	8.8	6.1	6.8	4.8	3.2	2.9	4.8	5.5	9.1	9.3	11.0
3.2	2.4	4.1	7.4	4.9		8.1	3.9	5.5	5.5	4.8	4.8	3.2	3.9	4.7	7.9	4.7	7.0	10.9	10.4	1.9

Fig. 15. *LS*-factors in the North and South Valleys.

As a basic variable of the *LS*-factor computation of the Shirasaka Watershed, the DEM had a resolution of 100 m^2 (10 × 10 m), which is shown in Figure 16. The slope inclination of a grid is a major variable for the slope steepness factor, whereas the spatial distribution of each grid was computed as the sine value ($\sin\theta$), which was multiplied by 1000 for convenience in the mapping process. Figure 17 shows the slope inclination map, where the upstream area has a higher inclination compared to the outlet and nearby grids downstream.

Figures 18 and 19 show the upstream slope area and length. These parameters belong to the group of *L*-factors for the computation of the *LS*-factor in the USLE. The upstream area increases downstream, and its location is near the depositional area along the foothills or along the line of the stream channel. Furthermore, the distribution of upstream length is also high in the downstream area, and on mountain ridges, it has a low value or a value equal to the length of a single grid. Both parameters of upstream area and upstream channel length are responsible for the accumulation of runoff for rill scouring to downstream areas.

Slope steepness (*S*) and slope length (*L*) are the sub-factors of the *LS*-factor, so both factors are equally responsible for the *LS*-factor (Figures 20 and 21). We excluded the grid along the stream channel (whose upstream area was >5000 m^2) and the flat area (slope <5%) as specified by the RUSLE. Although this exclusion algorithm is simple, it greatly affects the result of the averaged *LS* of the whole watershed.

3.1.4. Cover management factor (*C*)

The cover management factor is the ratio of soil loss from land cropped under specified conditions to the corresponding loss from clean tilled continuous fallow areas as defined by

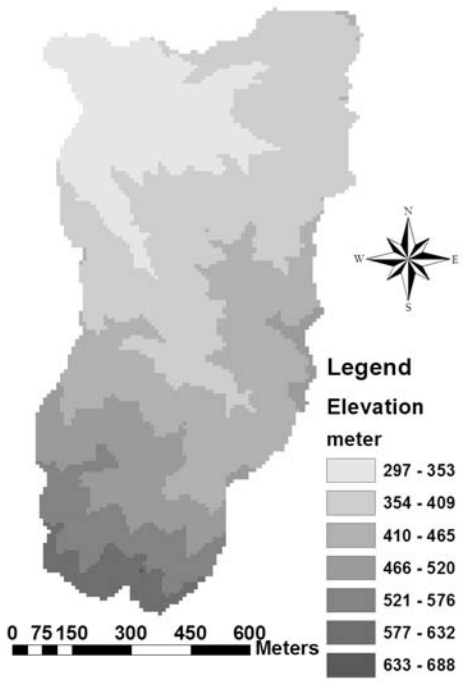

Fig. 16. Digital Elevation Model (DEM) of the Shirasaka Watershed

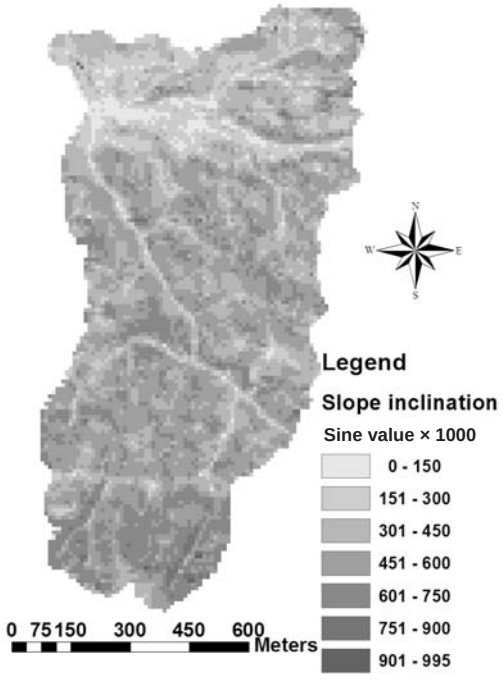

Fig. 17. Slope inclinations of the Shirasaka Watershed

WISCHMEIER and SMITH (1965). This factor is used in the USLE (and RUSLE) to reflect the effect of cropping and management practices on the erosion rate, and it is also often used to compare the relative effects of management options on conservation plans (RENARD *et al.* 1996). The major aspects in the calculation of the *C*-factor are the effects of previous cropping and management and the protection conferred to the soil surface by the vegetative canopy. Reduction of the *C*-factor occurs as a result of surface cover and surface roughness. In some cases, low soil moisture affects the reduction of runoff from low intensity rainfall.

For forested areas, there are three kinds of categories concerning the *C*-factor based on the condition of the forest and management practices: undisturbed forest, degraded forest (grazed, burned, or severely harvested), and reforestation area. Among these categories, the surface soil of undisturbed forest maintains a higher rate of infiltration, organic matter content, and high crown coverage of trees, duff coverage, or leaf litter. Such layers of duff shield the soil from the erosive force of runoff and raindrop impacts, which are extremely effective in soil erosion (WISCHMEIER and SMITH 1978).

In the Shirasaka Watershed, bare land was widespread 100 years ago because of repeated tree-cutting for fuel wood consumption by the ceramics industry. This situation changed after the establishment of the University Forest, and vegetation in this watershed has gradually attained

Table 2. *C*-factor for undisturbed forestland

Percent of area covered by canopy and understory	Percent of area covered by duff at least 50 mm deep	*C*-factor
100–75	100–90	0.0001–0.001
75–45	90–75	0.0020–0.004
45–20	75–40	0.0030–0.009

Source: WISCHMEIER and SMITH (1978)

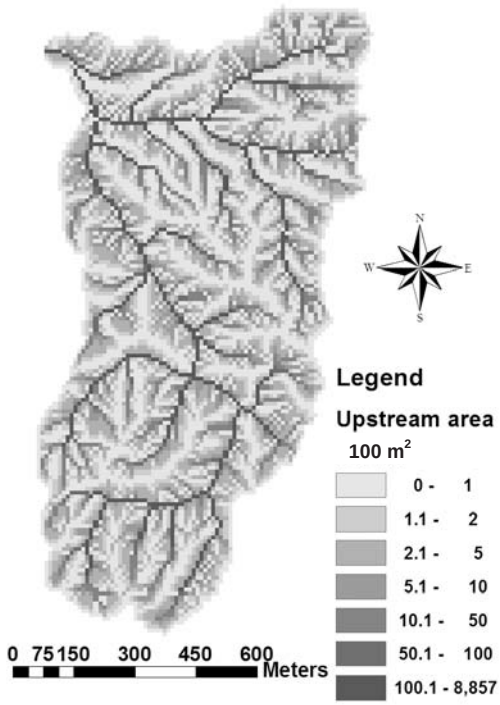

Fig. 18. Upstream areas of the Shirasaka Watershed

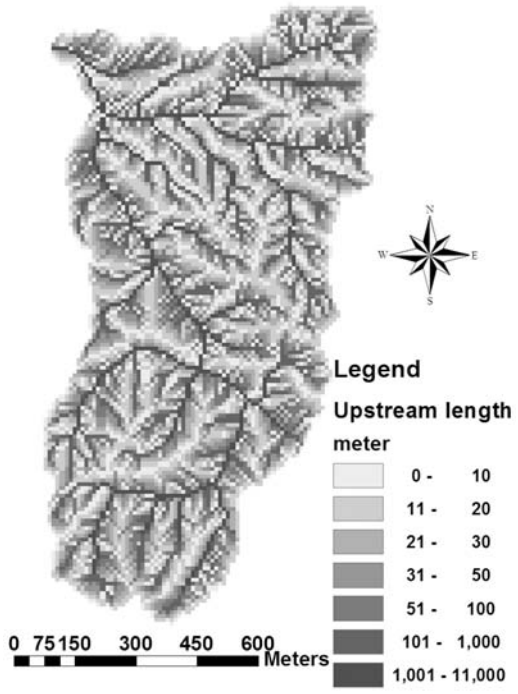

Fig. 19. Upstream lengths of the Shirasaka Watershed

crown closure (ARIYAKANON *et al.* 2000). Currently, the watershed resembles an undisturbed forested area, and crown coverage is very high, with three layers, i.e., upper canopy, mid-story, and forest floor. Furthermore, duff coverage of the forest floor caused by falling leaves is relatively high. Therefore, the nature of crown coverage and surface duff in the watershed is likely the same as in the proposed undisturbed forest of WISCHMEIER and SMITH (1978; Table 2). The estimated percentages of crown coverage and duff deposition based on a field survey of the Shirasaka Watershed were 75–100% and 90–100%, respectively.

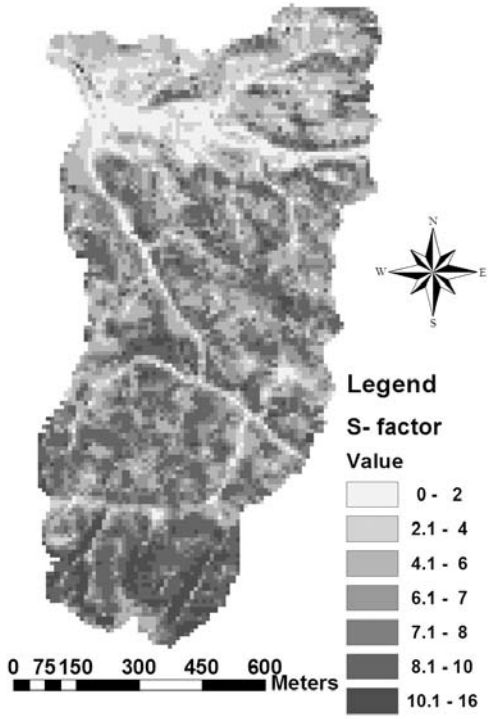

Fig. 20. *S*-factors of the Shirasaka Watershed

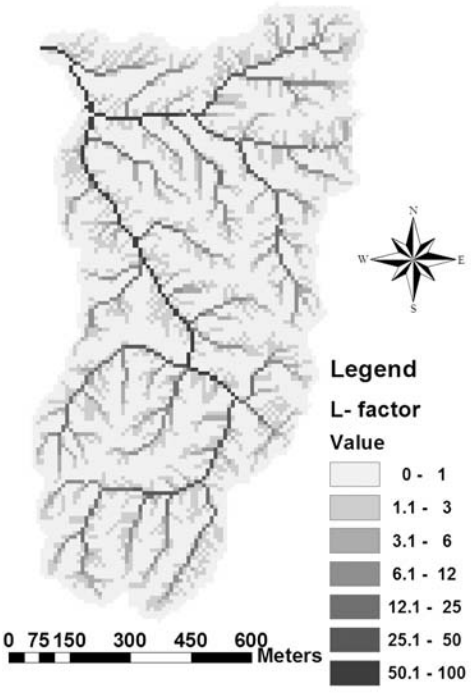

Fig. 21. *L*-factors of the Shirasaka Watershed

3.1.5. Support practice factor (*P*)

The support practice factor (*P*) is the ratio of soil loss with a specific support practice to the corresponding loss with upslope and downward slope tillage (WISCHMEIER and SMITH 1978). The *P*-factor in the USLE varies from 0 at minimum to 1 at maximum, based on the intensive use of different conservation practices. Materially improved tillage practices, sod-based rotations, treatment with fertilizers, and large quantities of crop residue left in the field can contribute to erosion control of cultivated land. These practices will slow water runoff and reduce the transportation capacity of a given amount of soil downslope of cultivated land.

The *P*-factor for natural conditions is 1 and decreases as the intensiveness of conservation measures against soil loss in watersheds increases. The present forested area of the Shirasaka Watershed was developed as an artificially treated slope because of previous land degradation. Through tree plantations, this watershed experienced intensive conservation support practices at the time of reforestation. The major activities were construction of check dams, gully plugging, hillside work, contouring, and terracing. However, some erosion control countermeasures are now around 50 years old, and many conservation efforts are disappearing beneath the forest stand, which now resembles a naturally regenerated forest. In general, the efficiency of any implemented foundation work decreases as the effect of reforestation increases over time, and

both should be evaluated as a time series (KITAHARA *et al.* 2000). The effectiveness of these foundation efforts has already ceased in their evaluation as a support practice factor in the USLE. Therefore, the *P*-factor used for the estimation of soil loss in the Shirasaka Watershed was that of a natural landscape.

3.2. Soil loss and sediment observations

3.2.1. Soil loss measurement in the small paired catchments

Soil loss observations in the small paired catchments were conducted at the outlets approximately once each month. The upper silting terrace, middle silting ditch, and lower silting reservoir were available as soil-loss observation facilities. Figure 22 shows an overview of the facilities.

The available sediment trap facility in these catchments differed from ordinary methods of event-wise soil loss measurements at the bottom of simple hillslopes. The deposited sediment of upper silting terraces was measured using a bucket; later, its volume was converted into the weight of soil lost. Differences in levels between present and previous measurements with reference to the water level were estimated for the lower silting reservoir and the middle silting

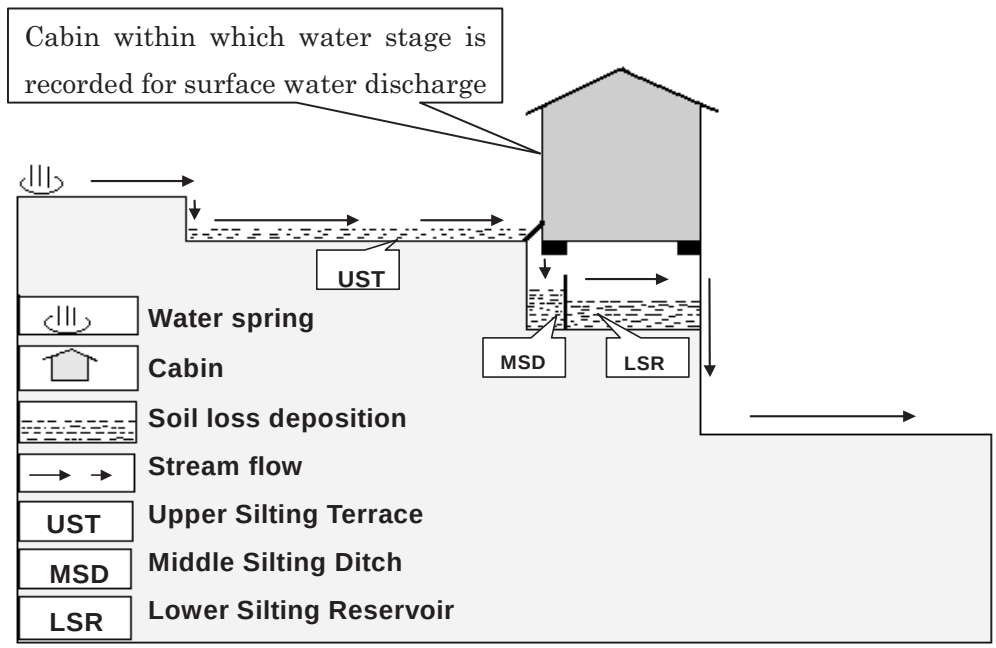

Fig. 22. Illustration of soil loss observations in the North and South Valleys
Note: Soil loss observation facilities were established at gauging stations for separate observations of surface water flow and groundwater flow. This figure only shows the profile of the surface water flow observation.

Fig. 23. Total load observation station at the Shirasaka Reservoir
Note: The total load is composed of all types of mass deposition, including soil loss.

ditch. The height of the notch at the water outlet of the reservoir was known, and the water level was measured using a point gauge. The measured volume [m^3] of the sediment was converted into weight [ton ha^{-1}] by multiplying by a conversion ratio, i.e., 1.44 ton m^{-3}. The period of sediment yield observations in these catchments was 4 years (9 August 2001 to 8 August 2005), and the total number of measurements was 42 over the whole period.

3.2.2. Total load measurement at the Shirasaka Reservoir

The deposited sediment was observed as the total load, i.e., bed load plus suspended load transported by stream water, at the Shirasaka Reservoir (Figure 23). The changing elevation of the sediment surface was detected by level surveying at the reservoir. Subtracting the newly surveyed level of the sediment surface from the previously measured level estimated the periodically deposited sediment yield of this watershed. In total, we made 25 observations of total load within this study period at intervals of about 1 week to 8 months.

The observed total load of the Shirasaka Reservoir was the product of all types of mass movement, including soil loss, that was generated on a mountain slope and passed downslope through the stream channel, and was ultimately deposited in the reservoir.

4. Results and discussion

The major objective of this study was to evaluate an appropriate model for the prediction of soil loss using an additional soil loss status map for a forested watershed underlain by weathered

Table 3. Reported annual soil loss of forested watersheds including estimated value

	Watershed name	Location	Country	Area km^2	Rainfall mm yr^{-1}	Memo	Soil loss ton ha^{-1} yr^{-1}	References
1	Upper Mahaweli watershed	Mahaweli river basin	Sri Lanka	3118	1800	Dense forest, comprise 11% of total watershed area	1	GUNATILAKE and GOPALKRISHNAN (1999)
2	Aandhi khola	Syngjha District Gandaki zone	Nepal	271	1650	Primary forest, 15.4% area of total watershed	2.2	PAHARI *et al.* (1996)
3	*National average*	Whole country	Nepal	147181	1300	Well managed forest	5–10	MPFS (1988)
4	Likhu khola	Nuwakot District Bagmati zone	Nepal	3.46	1850	Undisturbed forested plots (0.13 km^2)	0.3	SHRESTHA *et al.* (2003)
5	Sitlaro watershed	Dehradun Uttar Pradesh	India	52	1900	Average predicted value by USLE and Morgan Model for dense forest	1.57	JAIN *et al.* (2001)
6	Belgrad	Istanbul	Turkey	0.72	1094	Pseudo-maqui forested watershed (1)	**0.65**	OZAN *et al.* (2005)
				0.77		Pseudo-maqui forested watershed (2)	**0.62**	
				8×10^{-6}		Pseudo-maqui forested plot (1×8 m^2)	**0.1**	
7	Chomoli Garhwal	Uttar Pradesh	India	137.19	NM	Forest area only 24.16 km^2	**2.0–15**	WASSON (2003)
8	*Various plot*	Himalayan region	India Nepal	NM	NM	Measured sediment from plots and small catchments	**0.2– 1.5**	WASSON (2003)
9	Upper Ewaso	Ng'iro North basin	Kenya	15251	700	Naro moru gate (1)	**1**	MATI *et al*. (2000)
						Naro moru gate (2)	**1.3**	
10	Lawyers creek	Idaho	USA	544	533–737	Undisturbed forest area (9.069 km^2)	0.39	FERNANDEZ (2003)
11	Hawkesbury	Sydney NSW	Australia	0.02	907	Woodland/forest with a little grazing; Middle Triassic sandstone	**2**	ERSKAINE *et al.* (2002)
		Sydney NSW		0.05	1008		**3.1**	
		Sydney NSW		0.04	962		**4.2**	
12	Fool creek	Rocky mountain Colorado	USA	16	665	Logging and road construction	0.22	LEAF (1970)
	Dead horse creek	Rocky mountain Colorado		15		After 8 years	0.1	
	Lexen Creek	Rocky mountain Colorado		7		Later as uncut forest	0.05	

Note: NM: not mentioned
Soil loss: values expressed by bold numeric mean observed ones and others mean estimated values

granite. The soil loss observations, model validation, extension of the valid model to a large watershed, and the process of soil loss in the large watershed are discussed individually below.

4.1. Soil loss observations

Soil loss was observed in the North and South Valleys for 4 years (August 2001–August 2005), and the average soil loss in these catchments was around 0.6 ton ha^{-1} yr^{-1}. The observed soil loss in both small catchments was comparable to other areas with similar characteristics in the United States (MORGAN 1996), although the value of soil loss ranges from 0.05 to 0.5 ton ha^{-1} yr^{-1} in pre-cut forests (LEAF 1970). Table 3 shows the annual soil loss reported from various countries of the world. It shows that the soil loss in forested area where annual rainfall is about 1800 mm can be positioned between 0.3 and 15 ton ha^{-1} yr^{-1}. According to this result we can conclude that 0.6 ton ha^{-1} yr^{-1} as a value of soil loss in small paired catchments is significantly small. The main reason for the small soil loss in the catchments compared to degraded land in Japan (YOSHIKAWA *et al.* 2004) is the higher forest canopy coverage and accumulation of leaf litter. Another reason for the small soil loss in these catchments may be the lack of special mass movement processes such as gullies, landslides, stream bank cutting, or hillslope failures. Figure 24 shows the periodic soil loss observations in the North and South Valleys, indicating the relationship between rainfall patterns and soil losses in these catchments; however, concrete relationships cannot be explained fully because of the domination of other factors in the watershed. The soil loss in these valleys appeared to be very small or even negative in several events when there was no rainfall. The reason for this may be a lack of additional soil supplied to the reservoir and compaction of

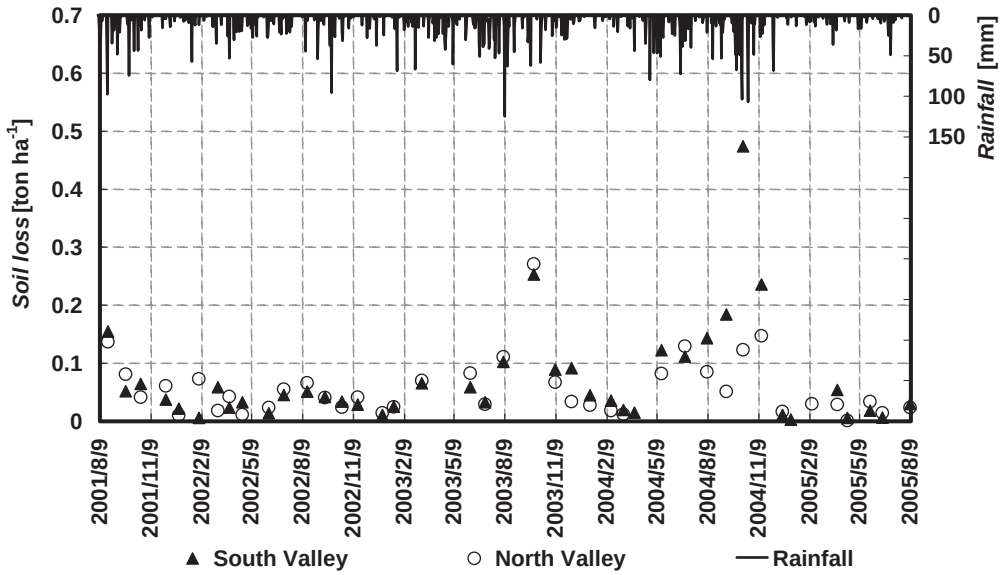

Fig. 24. Periodic soil loss observations in the North and South Valleys

previously deposited soil in the reservoir. In either case, these values have a negligible effect on the total quantity of soil loss.

A comparison of the observed soil loss in the North and South Valleys (Figure 24) shows that soil loss in the North Valley was higher than in the South Valley until the middle part of the study period, and the soil loss in the South Valley exceeded that in the North Valley after the winter of 2004. Moreover, the soil loss in the South Valley suddenly expanded more than five times the usual measurements in the summer of 2004, which was because of disturbance caused by the construction of a trail. However, consistent trends, such as decreasing or increasing soil loss over time, cannot be recognized only by considering the observed results.

4.2. Soil loss prediction and its goodness of fit

Soil loss in the North and South Valleys was predicted using the USLE and was compared to the observed soil loss in same catchments to test the applicability of the USLE.

4.2.1. Soil loss prediction

Soil loss in the North and South Valleys was predicted based on intensive rain events that exceeded 13 mm or 6 mm within a 15-min period during one event. The total number of events used for the prediction of soil loss was 132 for the study period, and we calculated the annual average value of the *R*-factor in the USLE as 4568 MJ mm ha^{-1} hr^{-1}. Temporal variations in soil loss were observed among events, seasons, and years because of the major effect of rainfall and

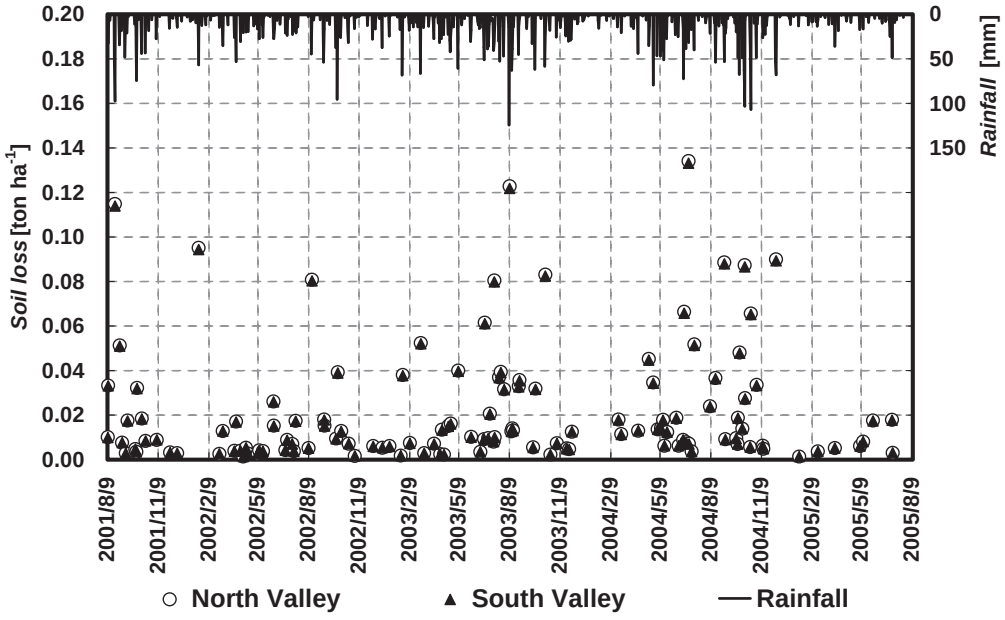

Fig. 25. Soil losses predicted during each rainfall event in the North and South Valleys

runoff in these catchments (Figure 25).

Topography is another influential factor for the spatial distribution of soil loss in each location. The main focus of this study was on this aspect, and we analyzed the slope length and steepness factor using a 10 × 10-m grid. Larger *L*- and *LS*-factors account for increased runoff volumes downslope. The *S*-factor accounts for increased runoff velocity in grids located on steep slopes. Therefore, the areas with the steepest inclination and the greatest length have the largest *LS*-factor in the USLE (DESMET and GOVERS 1996, MOLNAR and JULIAN 1997). In the same fashion, in the North and South Valleys, we found a higher *S*-factor for areas with a greater inclination and a lower *S*-factor for flatter areas.

The average spatial distribution of the *LS*-factor for the North and South Valleys was 8.27 and 8.02, respectively. The spatial distribution of the *LS*-factor in the North and South Valleys is shown in Figure 26. Table 4 shows the calculated value of all factors, which are used as multipliers for soil loss prediction in the USLE. The annual average predicted soil loss in the North and South Valleys was 0.701 and 0.696 ton ha^{-1} yr^{-1}, respectively (Table 5).

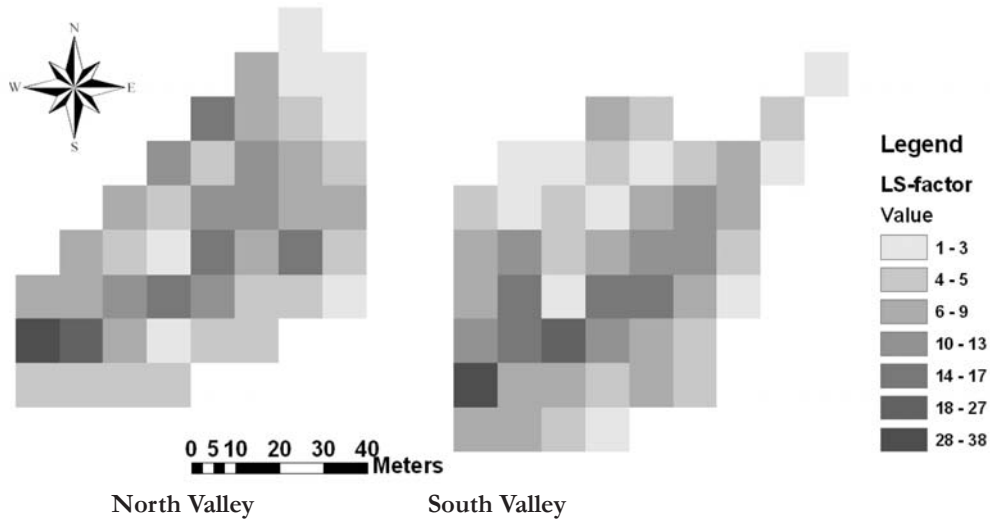

Fig. 26. Spatial distribution of the *LS*-factor in the North and South Valleys

Table 4. Soil loss factors of USLE in the North and South Valleys

Factors	Units	North Valley	South Valley	Remarks
Rainfall and runoff	MJ mm ha^{-1} hr^{-1}	4568	4568	Av. annual
Soil erodibility	ton hr MJ^{-1} mm^{-1}	0.019	0.019	
Slope length & steepness	Unitless	8.27	8.02	
Cover management	Unitless	0.001	0.001	
Support practice	Unitless	1	1	

Table 5. Annual predicted and observed soil loss in the North and South Valleys

Years		North Valley		South Valley		Rainfall [mm yr^{-1}]
		Predicted soil loss [ton ha^{-1} yr^{-1}]	Observed soil loss [ton ha^{-1} yr^{-1}]	Predicted soil loss [ton ha^{-1} yr^{-1}]	Observed soil loss [ton ha^{-1} yr^{-1}]	
First	(Aug. 2001~ Jul. 2002)	0.5610	0.4926	0.5569	0.5205	1532
Second	(Aug. 2002~ Jul. 2003)	0.7274	0.4469	0.7220	0.4603	1977
Third	(Aug. 2003~ Jul. 2004)	0.8988	0.6408	0.8922	0.9464	1818
Forth	(Aug. 2004~ Jul. 2005)	0.6157	0.4096	0.6112	*1.0390*	1553
Average	(Aug.2001~ Jul.2005)	0.7007	0.4975	0.6955	*0.7416*	1720

Note: value in italic is the result influenced by the artificial disturbance in catchment

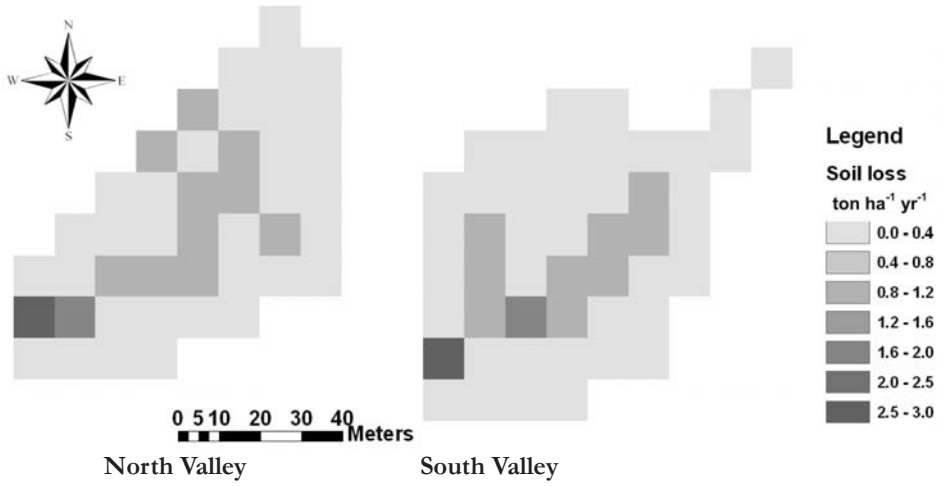

Fig. 27. Spatial distribution of predicted soil loss in the North and South Valleys averaged for August 2001 to July 2005

The *LS*-factor in the USLE appears to be largely responsible for the spatial variation in soil loss, especially for the area of homogeneous cover management and conservation practices. The spatial distribution of predicted soil loss in the North and South Valleys is shown in Figure 27.

A comparison of the predicted soil loss in the small paired catchments shows that soil loss was always greater in the North Valley than in the South Valley during the study period. The main reason for greater soil loss in the North Valley was the higher *LS*-factor, which may result from steeper slopes in the North Valley.

4.2.2. Goodness of fit

The soil loss observed at the outlets of the small paired catchments within this study period was

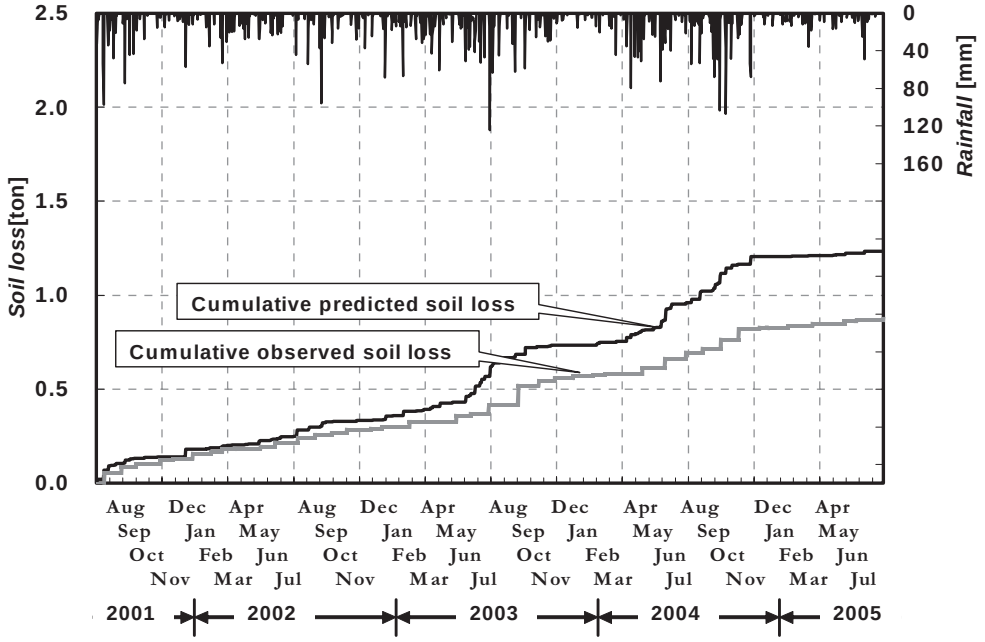

Fig. 28. Cumulative predicted and observed soil loss in the North Valley

0.876 and 1.424 tons for the North Valley and South Valley, respectively, and the total soil loss predicted by the USLE was 1.233 and 1.335 tons, respectively. In the North Valley, the predicted soil loss was very close to that observed until spring 2003 (Figure 28). With the summer rainfalls of 2003, this similarity disappeared until the following summer. The difference widened in June 2004, and ultimately, the predicted soil loss in the North Valley was greater than the observed value by 41%.

The cumulative predicted and observed soil loss in the South Valley is shown in Figure 29. In this valley, the cumulative predicted soil loss was 6% less than the observed soil loss, and this difference occurred suddenly in the latter part of the study period.

At the beginning of the study, the predicted soil loss was slightly higher than the observed loss. This situation reversed in the middle of the study period for several events. However, the difference between the observed and predicted soil loss in this catchment suddenly increased after September 2004. The main reason for the sudden increase in the observed soil loss was the treatment of the surface soil for improvement of the foot path and the stream channel in this catchment. Therefore, we conclude that the observed soil loss following the soil disturbances in this catchment were artificially increased. Only for the undisturbed period, the cumulative predicted soil loss was about 6.2% grater than the observed soil loss.

Table 5 shows the comparison of annual predicted and observed soil loss in both valleys with

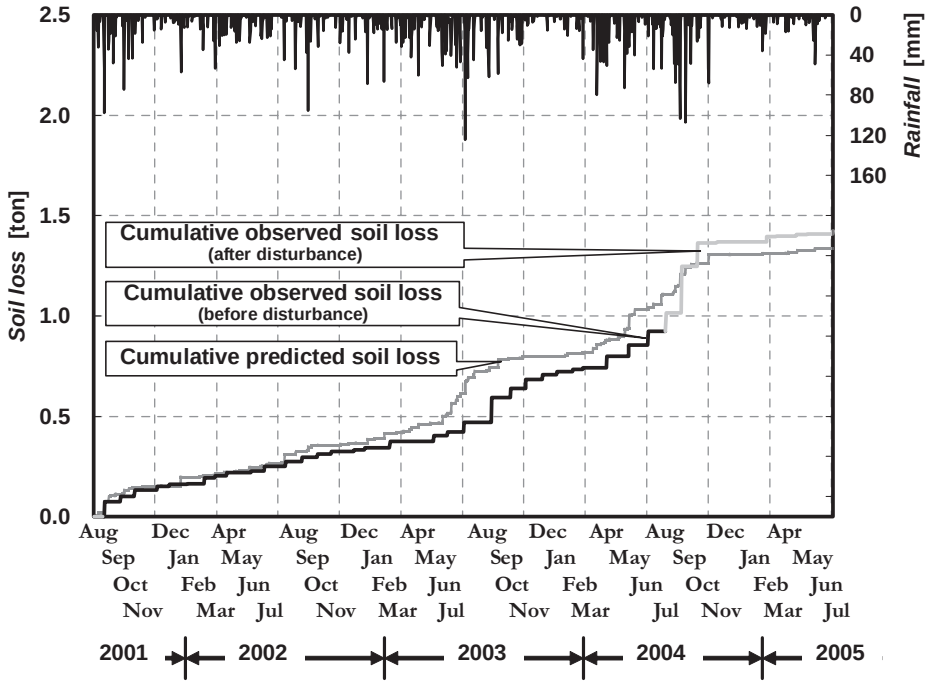

Fig. 29. Cumulative predicted and observed soil loss in the South Valley
Note: 1. On September 10, 2004 artificial disterbances occurred in South Valley
2. After the disterbance observed value is expressed in dotted grey line

annual rainfall trends. The information on annual soil loss indicates the trends in these catchments. Both predicted and observed soil losses were higher in the North Valley than in the South Valley.

The observed and predicted soil losses in the small paired catchments were well fitted, with some small differences. We therefore conclude that the USLE is highly applicable for the estimation of soil loss in a forested watershed underlain by deeply weathered granite.

4.3. Extension of the validated model to a large watershed

After testing its validity, we applied the USLE to the large watershed within the environment of the GIS and our drainage network algorithm. The Shirasaka Watershed is a large watershed that includes the North and South Valleys as paired small catchments. We therefore used the same factors as in the small paired catchments in the USLE, except *LS* (Table 6). More attention was given to the analysis of the *LS*-factor of this large watershed.

The *LS*-factor for the concave downstream area was found to be very high (>70) because of the higher inclination of the land surface with larger upstream area and length. The lowest value was calculated for the mountain ridge, where the slope inclination was low in some cases and the

Table 6. Characteristics of the Shirasaka Watershed

Characteristics	Units	Quantity	Remarks
Total load observation	ton ha^{-1} yr^{-1}	3.69	
Soil loss prediction	ton ha^{-1} yr^{-1}	0.94	
Rainfall and runoff factor	MJ mm ha^{-1} hr^{-1}	4567	Av. annual
Soil erodibility factor	ton hr MJ^{-1} mm^{-1}	0.019	
Slope length and steepness factor	Unitless	10.95	
Cover management factor	Unitless	0.001	
Support practice factor	Unitless	1	

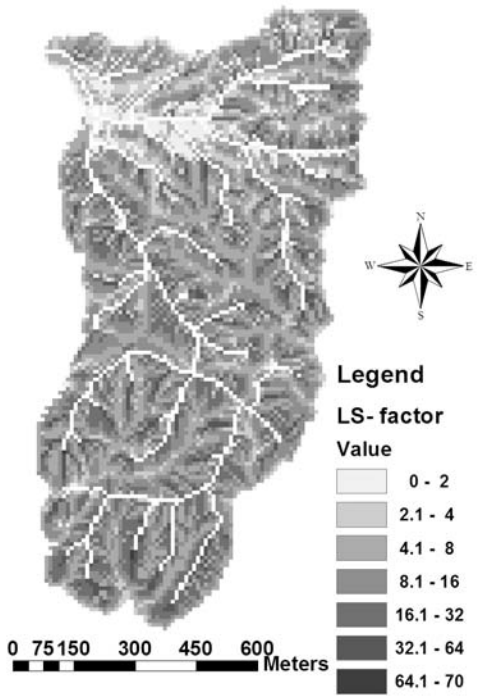

Fig. 30. Spatial distribution of *LS*-factor in the Shirasaka Watershed

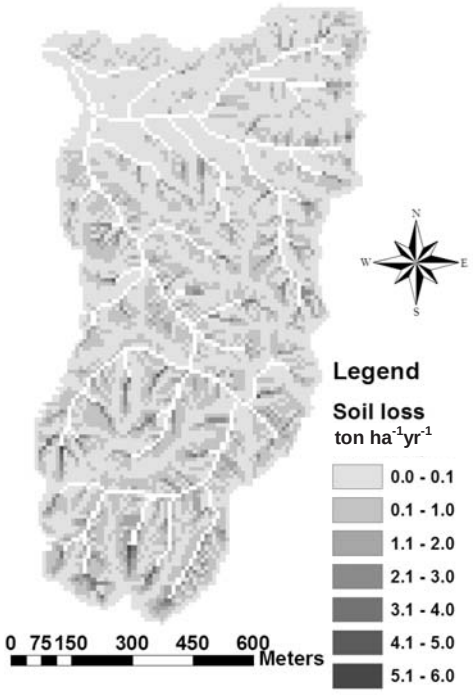

Fig. 31. Spatial distribution of predicted soil loss in the Shirasaka Watershed

upstream area and length were also small (Figure 30). In particular, the flat area ($\sin\theta < 0.05$) was excluded because of negligible erosion status or depositional area. The area of the stream channel was also excluded because this area was beyond the scope of the USLE.

Soil loss in the large watershed was calculated using the grid-based *LS*-factor, and the spatial distribution of soil loss was found to be high (>10 ton ha^{-1} yr^{-1}) and very low (0.01 ton ha^{-1} yr^{-1}), corresponding to areas with high and low *LS*-factors, respectively (recognizable in Figure 31).

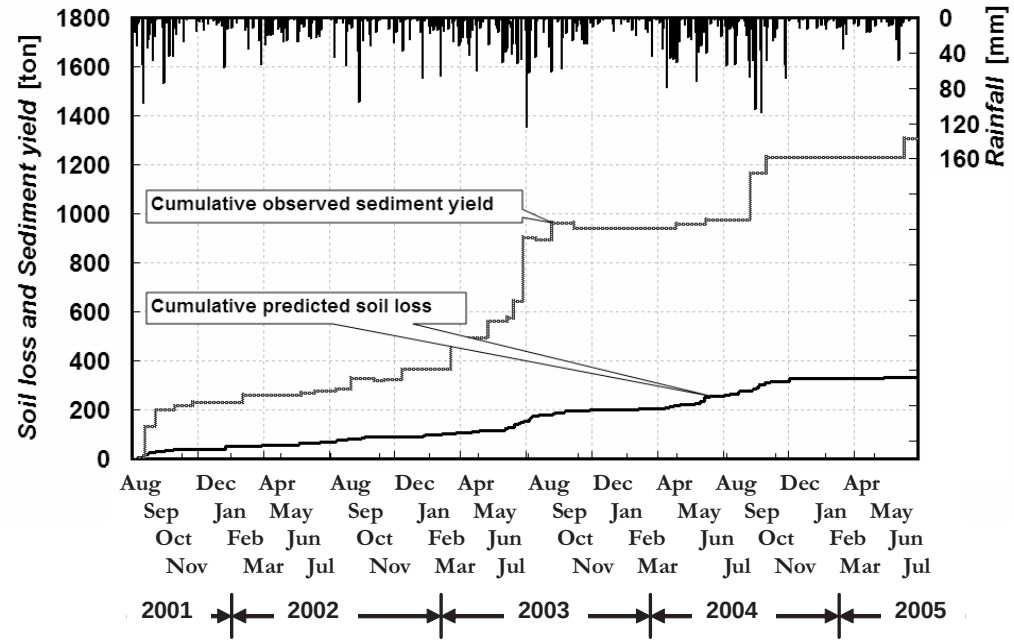

Fig. 32. Cumulative predicted soil loss and total load in the Shirasaka Watershed

Most of the observed sediment yield of the Shirasaka Reservoir is thought to have originated from various kinds of mass movement such as landslides, gullies, or stream bank failure. We compared the predicted soil loss and observed sediment yield of the Shirasaka Reservoir on the cumulative curve shown in Figure 32. The cumulative predicted soil loss and observed sediment yield of the Shirasaka Reservoir provide enough information to discuss watershed conditions under different soil erosion processes in the next section.

4.4. Soil loss processes in a large watershed

Soil erosion is a complex dynamic process by which surface soil is detached, transported, and accumulated elsewhere, and results in the depletion of surface soil productivity, subsurface soil exposure, and channel bed uplift. Sheet erosion, rill erosion, and gully erosion are step-wise series of soil loss processes from initial to advanced levels, and the level of advancement depends on the surface coverage and support practices in the watershed. Among these types of soil erosion processes, the estimation of soil loss by the USLE includes only the initial processes, i.e., sheet and rill erosion. However, these processes are no less important than gully erosion and mass movement along a river channel or landslides because of the nature of their occurrence on a plane throughout the watershed rather than along a line. The spatial distribution of average soil loss for four years is shown in Figure 31.

In the small paired catchments, the measurement of sediment yield as soil loss only considered

the yield of sheet and rill erosion. Likewise, the estimated soil loss of the Shirasaka Watershed also reflected only sheet and rill erosion because of the prediction limits of the USLE. However, the observed sediment yield of the Shirasaka Reservoir includes the sediment yield of all types of mass movement. The cumulative observed sediment yield at the reservoir is about four times greater than the cumulative predicted soil loss in this watershed (Table 6). Therefore, we assume that three-quarters of the sediment yield is the result of mass movement other than topsoil erosion from the watershed.

5. Conclusion

We developed a computational method to determine the *L*-factor based on a DEM and interpreted several variables concerning terrain attributes that were originally introduced by DESMET and GOVERS (1996). An algorithm to compute the inclination of a focal grid with regard to the *S*-factor was also modified to retain logic in interpreting the direction of the slope.

Goodness of fit was found to be very satisfactory between the observed and predicted soil loss in the small paired catchments (North and South Valleys), except for a short period during an artificial disturbance. This goodness of fit can be attributed to the appropriate estimation of the *LS*-factor in these small catchments, the *R*-factor based on reliable rainfall data, the *K*-factor based on laboratory tests for samples from these sites, and *C*- and *P*-factors based on suitable judgment of the watershed conditions. The extension of the results confirmed using the small paired catchments to a larger watershed through a DEM-based computational method was realistic, with reliable results in the soil loss estimation, because the generated maps of various factors did not appear to have any shortcomings.

Soil loss in the Shirasaka Watershed (estimated at 0.94 ton ha^{-1} $yr^{-}1$) was small compared to that of other watersheds in Japan, e.g., 12 ton ha^{-1} yr^{-1} in grassland and 40 ton ha^{-1} yr^{-1} in wild field (YOSHIKAWA *et al.* 2004). This was because of a higher percentage of canopy coverage and a thick layer of leaf litter coverage on the forest floor. Moreover, the lowest percentage of the smallest soil grain sizes (fine sand and silt: 33.7%; clay: 2.3%) and the domination of coarse grains (64%) in the surface soil was an additional factor that contributed to the small soil loss in this watershed (see Table 1).

Comparison of the predicted soil loss and observed reservoir deposition indicates that soil loss comprised about 25% of the sediment yield observed at the outlet of the watershed. The remaining 75% was attributed to mass movements that could not be calculated using the USLE.

Summary

We investigated soil loss in a forested watershed underlain by weathered granite to validate a method for estimating soil loss in mountainous regions based on parameter limitations and characteristics. For this purpose, we measured soil loss at the outlets of two small, paired catchments (North Valley, 0.44 ha; South Valley, 0.48 ha) and observed the total load of a large

watershed (Shirasaka Watershed, 88.6 ha) at a reservoir from August 2001 to July 2005. The study sites were located in the University Forest in Aichi, the University of Tokyo. Soil loss was predicted using the Universal Soil Loss Equation (USLE) and a drainage network calculation with a 10 × 10-m grid in a digital elevation model (DEM). The results were depicted using a Geographic Information System (GIS). The observed soil loss was 0.498 and 0.742 ton ha^{-1} yr^{-1} in the North and South Valleys, respectively. These values were small because of the weakening effect on raindrop energy of the thick litter layer and high crown coverage of the forest. Moreover, the small proportion of fine sediments, such as clay and silt, in the total soil materials also contributed to the low soil loss. The predicted values of soil loss showed a satisfactory goodness of fit to the observed values. Based on these results and information on the drainage network, we applied the same parameters of the USLE to the Shirasaka Watershed and calculated an average soil loss of 0.940 ton ha^{-1} yr^{-1} over 4 years. High soil loss was evident on the lower parts of slopes, on concave slopes, and in the foothills just before the depositional area because of the effects of highly accumulated surface runoff. A comparison of observed total sediment yield in the reservoir (3.69 ton ha^{-1} yr^{-1}) and predicted soil loss from the Shirasaka Watershed indicated that the ratio of soil loss to total sediment yield was about 25%; the remainder was attributed to other types of mass movement.

Key words: Drainage Network, Forested Watershed, Universal Soil Loss Equation, Weathered Granite

References

ARIYAKANON, N., NUMAMOTO, S., SUZUKI, M. (2000) Sixty-year decreasing trend of bare land in the Shirasaka Watershed, University Forest in Aichi, revealed by aerial photography. Bulletin of Tokyo University Forests 103, 103-339

COHEN, M.J., SHEPHERD, D.K., WALSH, M.G. (2005) Empirical reformulation of the universal soil loss equation for erosion risk assessment in a tropical watershed. Geoderma 124, 235-252

DESMET, P.J.J., GOVERS, G. (1996) A GIS procedure for automatically calculating the USLE LS factor on topographically complex landscape units. Journal of Soil and Water Conservation 51, 427-433

ERSKAINE, W.D., MAMOULDZADEH, A., MYERS, C. (2002) Land use effect on sediment yield and soil loss rate in small basin of Trassic sandstone near Sydney, NSW, Australia. CATENA 49, 271-287

FERNANDEZ, C., WU, J.Q., MCCOOL, D.K., STOCKLE, C.O. (2003) Estimating water erosion and sediment yield with GIS, RUSLE, and SEDD. Journal of Soil and Water Conservation 58, 128-136

FOSTER, G.R., WISCHMEIER, W.H. (1974) Evaluating irregular slopes for soil loss prediction. Transactions of the American Society of Agricultural Engineers 17, 305-309

GUNATILAKE H.M., GOPALKRISHNAN C. (1999) The economics of Reservoir sedimentation: A case study of Mahaweli Reservoir in Sri Lanka. Water Resource Development, Volume 4, 511-526

JAIN, S.K., KUMAR, S., VERGHESE, J. (2001) Estimation of soil erosion for a Himalayan watershed using GIS technique. Water Resource Management 15, 41-54

KIMOTO, A. (2003) Soil erosion and human impacts in hilly devastated granite mountains. Ph.D. Dissertation, 102pp, Kyoto University, Japan

KINNELL, P.I.A. (1997) Converting USLE soil erodibility for use with the QR EI30 index. Soil and Tillage Research 45, 349-357

KITAHARA, H., OKURA, Y., SAMMORI, T., KAWANAMI, A. (2000) Application of the Universal Soil Loss Equation (USLE) to mountainous forests in Japan. Journal of Forest Research 5, 231-236

LEAF, C.F. (1970) Sediment yields from central Colorado, Snow zone. Journal of the Hydraulic Division ASCE 96, 87-93

MATI, B.M., MORGAN, R.P.C., GICHUKI, F.N., QUINTON, J., BREWER, T.R., LINIGER, H.P. (2000) Assessment of erosion hazard with the USLE and GIS: A cause study of the upper Ng'iro North basin of Kenya. Journal of Applied Genetics (JAG), 2, 2

MFSC: Master Plan for Forestry Sector Nepal. *In* Soil Conservation and Watershed Management Plan. MFSC (Ministry of forestry & soil concervation), 184pp, Kathmandu, Nepal, 1988

MOLNAR, D.K., JULIAN P.Y. (1997) Estimation of upland erosion using GIS. Computer and Geoscience 24, 183-192

MORGAN, R.P.C. (1996) Soil Erosion and Conservation (Second Edition), Longman, 164 pp

MOROTO, K., YOSHIHISA, M., HARUTA, Y. (1978) Soil properties and growth of Japanese red pine (*Pinus densiflora*) in the hilly and low-mountainous region of central Japan. Journal of Japanese Forestry Society 69, 371-378 (in Japanese with English summary)

ODURO-AFRIYIE, K. (1996) Rainfall erosivity map of Ghana. Geoderma 74, 161-166

OZAN, S., NIGAT B.A., OZYUVACI, N., HIZAL, A., GOKBULAK, F., SERINGEL, Y. (2005) Cover and management factor for the Universal Soil loss Equation for forest ecosystems in the marmara region, Turkey. Forest Ecology and Management 214, 118-123

PAHARI, K., DELSOL J.P., MURAI, S. (1996) Paper presented at the 4th International Symposium on High Mountain Remote Sensing Cartography, Karlstad - Kiruna - Tromsø, August 19-29

RENARD, K.G., FOSTER, G.R., WEESIES, G.A., MACCOOL, D.K., YODER, D.C. (1996) Predicting Soil Erosion by Water: A Guide to Conservation Planning with the Revised Universal Soil Loss Equation (RUSLE). Agricultural Handbook Number 703, USDA 384

RENARD, K.G., FOSTER, G.R., WEESIES, G.A., PORTER, J.P. (1991) RUSLE Revised Universal Soil Loss Equation. Journal of Soil and Water Conservation 46, 30-33

SHIBANO, H. (1998) Effects of Forest Regeneration on the Water Budget of Small Catchments in Mountains of central Japan. *In* Haigh, M.J., J. KRECEK, G.S. RAJWAR, and M.P. KILMARTIN (eds). Headwaters – water resources and soil conservation–: Proceedings of Headwater '98, the Fourth International Conference on Headwater Control, Merano, Italy, 273-282

SHRESTHA, D.P., ZINCK, J.A., RANST, E.V. (2003) Modeling land degradation in the Nepalese Himalaya. CATENA 57, 135-156

WASSON, R.J. (2003) A sediment budget for the Ganga – Brahmaputra catchment. Current Science 84, 8

WISCHMEIER, W.H., SMITH, D.D. (1965) Predicting Rainfall Erosion Losses from Crop Land East of the Rocky Mountains –Guide for Selection of Practice for Soil and Water Conservation–. *In* Agricultural Handbook, USDA, 1-47

WISCHMEIER, W.H., SMITH, D.D. (1978) Predicting Rainfall Erosion Losses –A Guide to Conservation Planning– *In* Supersedes Agriculture Handbook No. 282, "Predicting Rainfall Erosion Losses from Cropland East of the Rocky Mountains", United States Department of Agriculture in cooperation with Purdue Agricultural Experiment Station, 1-58

YAMAGUCHI, I. (1963) Fundamental Studies on the Groundwater Flow Phenomena at the Water Source Zone. Bulletin of the Tokyo University Forests 58, 133-285

YOSHIKAWA, S., YAMAMOTO, H., HANANO, Y., ISHIHARA, A. (2004) Hilly-land Soil Loss Equation (HSLE) for evaluation of soil erosion caused by the abandoned agricultural practices. Japan Agricultural Research Quarterly 38, 21-29

（Received Sep. 2, 2005）
（Accepted Jan.10, 2006）

風化花崗岩上に成立した森林流域からの土壌表層侵食 －GISに依拠したUSLE式による予測値と観測値の比較－

クリシュナ　バハドゥール　カルキ*1 • 芝野博文*2

*1 東京大学大学院農学生命科学研究科生圏システム学専攻
*2 東京大学大学院農学生命科学研究科附属演習林愛知演習林

要　　旨

風化花崗岩上に成立した森林流域からの土壌表層侵食の特性とそれを表現するモデルのパラメータとを検討した。調査地は，東京大学愛知演習林の白坂試験流域 88.6 ha とその内部の北谷 0.44 ha と南谷 0.48 ha であり，調査期間は，2001 年 8 月から 2005 年 7 月までである。土壌表層侵食は，DEM を用いて一辺 10 m の正方形に区分した格子点から形成される流路網を特定し，これに USLE 式を応用した後，GIS によりその空間分布を表現した。観測された土壌表層侵食量は，北谷で 0.498 ton ha^{-1} yr^{-1} であり，南谷で 0.742 ton ha^{-1} yr^{-1} であった。この低い値は，一つには雨滴のエネルギーに対して樹冠や落葉層による緩衝が要因だが，他方では微細な粒径の堆積物即ち粘土やシルトの占める比率が全侵食量に対して小さかったこともその要因である。予測値は観測値に対して満足のいく結果を示した。この結果を踏まえ，同一のパラメータと流路網の情報を用いて白坂試験流域へ拡張したところ，0.940 ton ha^{-1} yr^{-1} が計算された。空間分布でみると，高い土壌表層侵食は山腹（集水域のうちモデルが表現できる上限を超えない範囲で）の下端や凹面形状の斜面あるいは（勾配が緩くなり）堆積が発生する直前の山腹の基部に見られ，表面流出が集積する効果と見られた。白坂試験流域の貯水池で観測された全流出土砂量の観測結果(3.69 ton ha^{-1} yr^{-1}) に占める推定値である土壌表層侵食量の比率は，25％程度となり，残りの 75％は，土壌表層侵食とは別のマスムーブメントに起因していると結論付けられた。

キーワード： 流路網・森林流域・USLE・風化花崗岩